Article

Cell Reports

Blimp1 Prevents Methylation of *Foxp3* and Loss of Regulatory T Cell Identity at Sites of Inflammation

Graphical Abstract

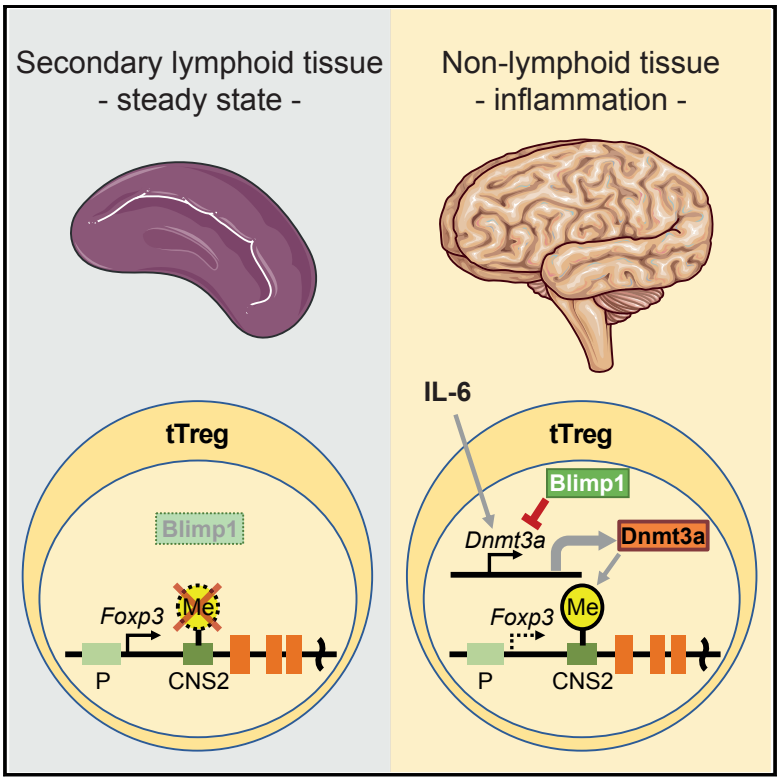

Authors

Garima Garg, Andreas Muschaweckh, Helena Moreno, ..., Jochen Huehn, Axel Kallies, Thomas Korn

Correspondence

thomas.korn@tum.de

In Brief

An inflammatory environment threatens the stability of Foxp3^{+} Treg cells. Garg et al. show that by expressing the transcriptional regulator Blimp1, Treg cells resist the IL-6-driven loss of Foxp3 in inflamed tissues. Blimp1 prevents the methylation and reduced expression of *Foxp3* through inhibition of the methyltransferase Dnmt3a.

Highlights

- Most Foxp3^{+} Treg cells in the inflamed CNS express Blimp1
- Blimp1 inhibits Dnmt3a and prevents methylation of the *Foxp3* locus
- IL-6 contributes to methylation of the *Foxp3* locus in a Dnmt3a-dependent manner
- Blimp1 counteracts the IL-6-driven destabilization of Treg cells

Garg et al., 2019, Cell Reports *26*, 1854–1868
February 12, 2019
https://doi.org/10.1016/j.celrep.2019.01.070

CellPress

OPEN ACCESS
CellPress

Cell Reports
Article

Blimp1 Prevents Methylation of *Foxp3* and Loss of Regulatory T Cell Identity at Sites of Inflammation

Garima Garg,[1] Andreas Muschaweckh,[1] Helena Moreno,[2] Ajithkumar Vasanthakumar,[3,4] Stefan Floess,[5] Gildas Lepennetier,[1] Rupert Oellinger,[6,7] Yifan Zhan,[3,4] Tommy Regen,[8] Michael Hiltensperger,[1] Christian Peter,[1] Lilian Aly,[1,9] Benjamin Knier,[1] Lakshmi Reddy Palam,[10] Reuben Kapur,[10] Mark H. Kaplan,[10] Ari Waisman,[8] Roland Rad,[6,7] Gunnar Schotta,[2] Jochen Huehn,[5] Axel Kallies,[3,4] and Thomas Korn[1,9,11,*]

[1]Klinikum Rechts der Isar, Department of Experimental Neuroimmunology, Technical University of Munich, Ismaninger Str. 22, 81675 Munich, Germany

[2]Biomedical Center (BMC) and Center for Integrated Protein Science Munich, Faculty of Medicine, LMU Munich, Grosshaderner Str. 9, 82152 Planegg-Martinsried, Germany

[3]The Peter Doherty Institute for Infection and Immunity, University of Melbourne, 792 Elizabeth St., Melbourne Victoria 3000, Australia

[4]The Walter and Eliza Hall Institute of Medical Research, 1G Royal Parade, Parkville, Victoria 3052, Australia

[5]Experimental Immunology, Helmholtz Centre for Infection Research, Inhoffenstr. 7, 38124 Braunschweig, Germany

[6]Institute of Molecular Oncology and Functional Genomics, TranslaTUM Cancer Center, Technical University of Munich, Ismaninger Str. 22, 81675 Munich, Germany

[7]Klinikum Rechts der Isar, Department of Medicine II, Technical University of Munich, Ismaninger Str. 22, 81675 Munich, Germany

[8]Institute for Molecular Medicine, University Medical Center of the Johannes Gutenberg University of Mainz, Langenbeckstr. 1, 55131 Mainz, Germany

[9]Munich Cluster for Systems Neurology (SyNergy), Feodor-Lynen-Str. 17, 81377 Munich, Germany

[10]Herman B. Wells Center for Pediatric Research, Department of Pediatrics, Indiana University School of Medicine, 1044 West Walnut St., Indianapolis, IN 46202, USA

[11]Lead Contact

*Correspondence: thomas.korn@tum.de

https://doi.org/10.1016/j.celrep.2019.01.070

SUMMARY

Foxp3$^+$ regulatory T (Treg) cells restrict immune pathology in inflamed tissues; however, an inflammatory environment presents a threat to Treg cell identity and function. Here, we establish a transcriptional signature of central nervous system (CNS) Treg cells that accumulate during experimental autoimmune encephalitis (EAE) and identify a pathway that maintains Treg cell function and identity during severe inflammation. This pathway is dependent on the transcriptional regulator Blimp1, which prevents downregulation of Foxp3 expression and "toxic" gain-of-function of Treg cells in the inflamed CNS. Blimp1 negatively regulates IL-6- and STAT3-dependent Dnmt3a expression and function restraining methylation of Treg cell-specific conserved non-coding sequence 2 (CNS2) in the *Foxp3* locus. Consequently, CNS2 is heavily methylated when Blimp1 is ablated, leading to a loss of Foxp3 expression and severe disease. These findings identify a Blimp1-dependent pathway that preserves Treg cell stability in inflamed non-lymphoid tissues.

INTRODUCTION

Foxp3$^+$ Treg cells are either thymus derived (tTreg cells) or induced from conventional CD4$^+$ T (Tconv) cells outside the thymus (pTreg cells) or can be generated *in vitro* (iTreg cells) (Abbas et al., 2013). In an inflamed environment, such as the CNS during experimental autoimmune encephalomyelitis (EAE), pTreg cells cannot be generated and tTreg cells migrate to the CNS, become activated in a T cell receptor (TCR)-dependent manner, expand, and acquire suppressive Treg effector functions (Korn et al., 2007; O'Connor et al., 2007). Even though tTreg cells are indispensable to control CNS inflammation (McGeachy et al., 2005), little is known about their resilience to inflammation in the CNS.

Epigenetic DNA marks are crucial determinants of Treg cell identity. Complete demethylation of the conserved non-coding sequence 2 (CNS2), also known as Treg cell-specific demethylated region (TSDR), in the first intron of the *Foxp3* locus is required for optimal expression of Foxp3 (Floess et al., 2007). Conversely, methylation of CNS2 results in the reduced transcription of *Foxp3* and subsequent loss of Treg cell functionality. Notably, less demethylation of CNS2 in iTreg cells causes their instability compared to tTreg cells (Polansky et al., 2008). While epigenetic manipulation is intensely explored to "stabilize" iTreg cells (also for therapeutic use), less is known about modifications of epigenetic DNA marks in tTreg cells. Interestingly, CNS2 demethylation in tTreg cells is already initiated during thymic development (Toker et al., 2013), in a process that appears independent of the induction of Foxp3 (Ohkura et al., 2012). Therefore, impaired DNA demethylation in tTreg cells might compromise their identity in spite of a fully mounted Foxp3-dependent transcriptional program.

Blimp1 is a zinc finger protein, which serves as a transcriptional regulator and is indispensable for the development of

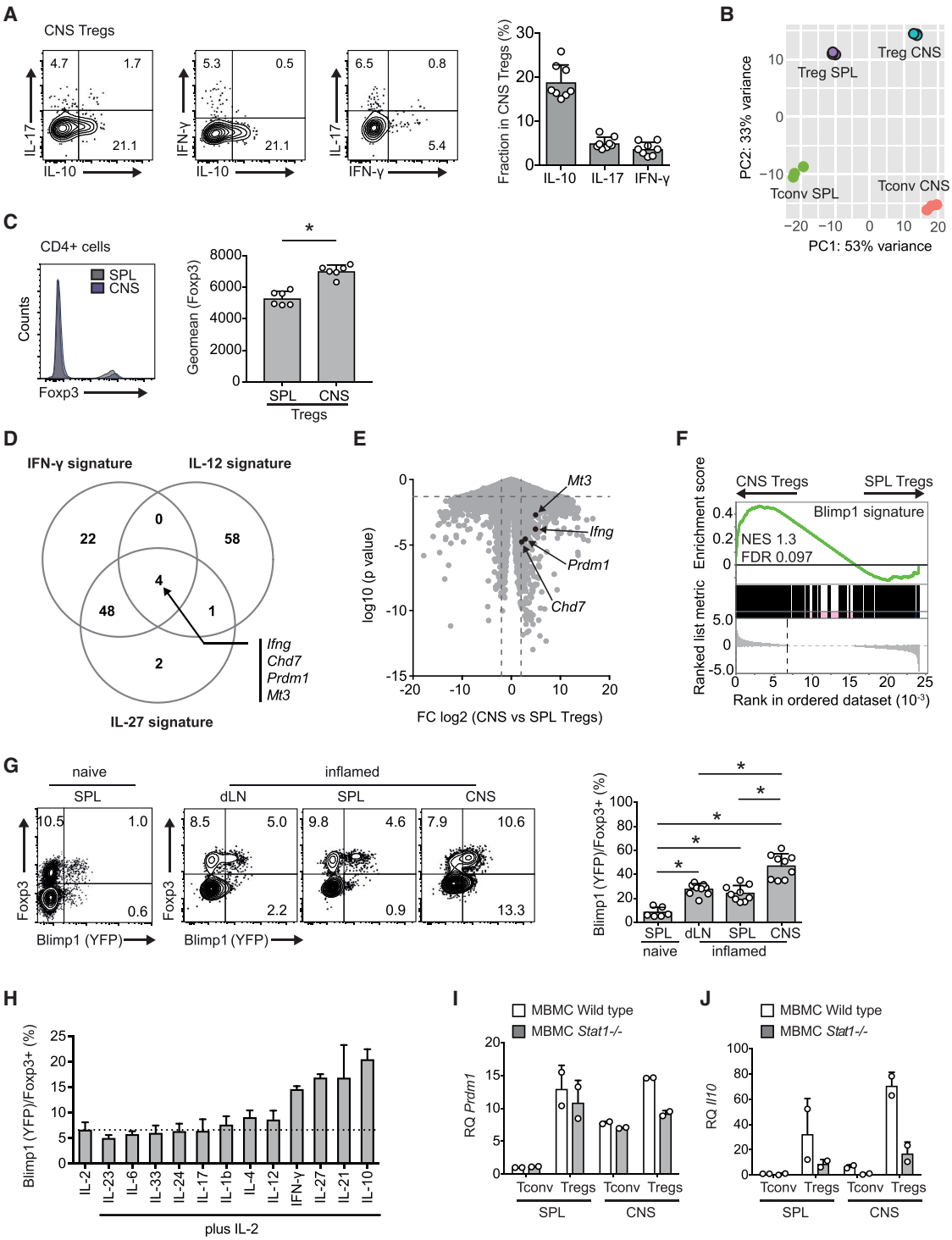

Figure 1. CNS Treg Cells are Stable and Express Blimp1 in Response to Proinflammatory Cytokines

(A) Mononuclear cells were isolated from the CNS of EAE mice at the peak of disease and were stimulated with phorbol 12-myristate 13-acetate (PMA) and ionomycin to analyze the expression of IL-10, IL-17, and IFN-γ in Treg cells by flow cytometry. Mean of eight biological replicates ± SD, derived from three independent experiments. Symbols depict individual mice (bars, mean ± SD).

(B) $CD4^+Foxp3^+$ Treg cells were sorted from the CNS and spleen (SPL) of Foxp3 (GFP) reporter mice at the peak of EAE and subjected to RNA-seq. Principal-component analysis.

(legend continued on next page)

plasma cells and fully functioning effector CD8$^+$ T cells (Kallies et al., 2009; Rutishauser et al., 2009; Shapiro-Shelef et al., 2003). In CD4$^+$ T cells, Blimp1 limits follicular helper T cell differentiation (Choi et al., 2011). Furthermore, Blimp1 transactivates *Il10* and thereby drives the conversion of T helper 1 (Th1) and Th17 cells into type 1 regulatory T (Tr1) cells (Heinemann et al., 2014; Neumann et al., 2014). Finally, Blimp1 has been identified to support a residency program of CD8$^+$ T cells in non-lymphoid tissues (Mackay et al., 2016). In Treg cells, Blimp1 cooperates with interferon regulatory factor 4 (IRF4) to establish a Treg cell effector program, including the expression of interleukin-10 (IL-10) and granzyme B in particular in non-lymphoid tissues (Cretney et al., 2011; Vasanthakumar et al., 2015).

Here, we reveal a non-redundant function for Blimp1 in preserving the identity of Treg cells, particularly under conditions of an inflammatory challenge. IL-6 signaling induces and activates the DNA methylating enzyme Dnmt3a, which is mounted to distinct DNA sites in the absence of Blimp1, leading to CNS2 methylation and Foxp3 downregulation. Conversely, Blimp1 inhibits the upregulation of *Dnmt3a*, prevents methylation of CNS2 in the *Foxp3* locus, and thereby maintains Treg cell identity and function. Consequently, Treg cell-specific loss of Blimp1 in an inflammatory environment results in the methylation of CNS2, loss of Foxp3 expression, and the acquisition of a proinflammatory T cell phenotype.

RESULTS

Treg Cells Show Stable Foxp3 Expression in the Inflamed CNS *In Vivo*

Strong inflammation can trigger the loss of Treg cell identity and acquisition of a proinflammatory phenotype in Treg cells (Zhou et al., 2009). Consistent with earlier reports (Kim et al., 2017; Korn et al., 2007), CNS Treg cells during EAE did not only express IL-10, but a fraction of them expressed proinflammatory cytokines, including IL-17 and interferon-γ (IFN-γ) (Figure 1A). In RNA sequencing (RNA-seq) analysis of Foxp3 (GFP)$^+$ Treg cells isolated from the spleen and CNS of EAE mice at the peak of disease, CNS Treg cells showed a downregulation of 507 genes and upregulation of 783 genes (>2-fold, $p < 0.05$) as compared with splenic Treg cells, together comprising a transcriptional signature of CNS Treg cells (Table S1). As expected, principal-component analysis (PCA) showed that splenic and CNS Treg cells grouped together in principal component 2 (PC2) and clearly separated from conventional CD4$^+$ T cells isolated from the same organs (Figure 1B). Interestingly, however, principal component 1 (PC1) separated these populations according to the organ they were isolated from, indicating that the tissue controls significant parts of the transcriptional signature (Figure 1B). Notably, signature genes of Th1 and Th17 genes were upregulated in CNS Treg cells as compared to splenic Treg cells (Figures S1A and S1B). Thus, at the site of inflammation, Treg cells appeared to be poised for proinflammatory effector programs. However, Foxp3 was maintained in CNS Treg cells and expressed in even higher amounts than in splenic Treg cells during disease (Figure 1C). Thus, we hypothesized that specific mechanisms must exist that preserve Treg cell identity in an inflamed environment.

CNS Treg Cells Express High Amounts of Blimp1 and Display an Effector Treg Cell Signature

Proinflammatory cytokines have been implicated both in the maintenance and loss of Treg cell identity (Koch et al., 2012; Overacre-Delgoffe et al., 2017). To understand which pathways may have an impact on Treg cells during CNS inflammation, we performed gene set enrichment analyses in CNS versus splenic Treg cells. CNS Treg cells showed pronounced enrichment for IFN-γ-, IL-12-, and IL-27- (but not IL-23, data not shown) induced genes, suggesting that CNS Treg cells can sense multiple inflammatory cytokines during inflammation (Figure S1C). Notably, *Prdm1* (encoding Blimp1) was common to all three gene sets (Figures 1D and 1E). Blimp1 expression was higher in CNS Treg cells compared to splenic Treg cells, and effector Treg cell signature genes expressed in Blimp1$^+$ versus Blimp1$^-$ Treg cells (Cretney et al., 2011) were highly enriched in the transcriptional profile of CNS as compared to splenic Treg cells (Figure 1F).

Using a Blimp1 (yellow fluorescent protein [YFP]) reporter mouse (Rutishauser et al., 2009), we confirmed that the majority of Foxp3$^+$ Treg cells were Blimp1 (YFP)$^+$ in the inflamed CNS, whereas the fraction of Blimp1 (YFP)$^+$ Treg cells was only about 10% in the spleen in steady state (Figure 1G). Taken together, Treg cells that accumulated in the inflamed CNS displayed a distinct transcriptional signature characterized

(C) Foxp3 expression by intracellular staining of splenic Treg cells and CNS Treg cells at the peak of EAE. Mean of six biological replicates ± SD, derived from two independent experiments. Symbols depict individual mice (bars, mean ± SD), t test, $p < 0.00005$.
(D and E) Enrichment of CNS Treg "signature" genes in gene sets upregulated in T cells in response to IL-12 (Agarwal et al., 2009) or IL-27 or IFN-γ (Hall et al., 2012). Overlap of core enriched genes of the IL-12, IL-27, and IFN-γ signatures in CNS Treg cells as venn diagram (D) and volcano plot (E).
(F) Enrichment of Blimp1 signature genes (Cretney et al., 2011) within CNS Treg cells and spleen Treg cells.
(G) Blimp1 expression was analyzed within Foxp3$^+$ cells in naive spleen and in indicated compartments at the peak of EAE in Blimp1 (YFP) reporter mice. Fraction of Blimp1 (YFP)$^+$ cells in Treg cells, mean of nine biological replicates ± SD, derived from three independent experiments. Symbols depict individual mice (bars, mean ± SD). Significance was calculated using ANOVA plus Tukey's post test, $p < 0.05$.
(H) Cytokines inducing Blimp1 in Treg cells *in vitro*. CD4$^+$CD25$^+$GITR$^+$Blimp1 (YFP)$^-$ Treg cells were sorted from the spleen and lymph nodes (LNs) of naive Blimp1 (YFP) reporter mice and cultured with anti-CD3 and anti-CD28 dynabeads in the presence of the indicated cytokines. On day 4, Blimp1 (YFP) expression was analyzed by flow cytometry. Data are summarized from two independent experiments (three technical replicates per experiment) (mean ± SD).
(I and J) Blimp1 is induced in a STAT1-dependent manner *in vivo*. Tconv and Treg cells were fluorescence-activated cell sorting (FACS) sorted from the spleen and CNS of immunized mixed bone marrow chimeras generated with wild-type plus *Stat1*$^{-/-}$ bone marrow. The expressions of *Prdm1* (encoding Blimp1) (I) and *Il10* (J) in Tconv and Treg cells were analyzed by qPCR of re-sorted congenically marked control and knockout cells. Data were summarized from two independent biological replicates. Symbols depict individual biological replicates (bars, mean ± SD).
See also Figures S1 and S2 and Table S1.

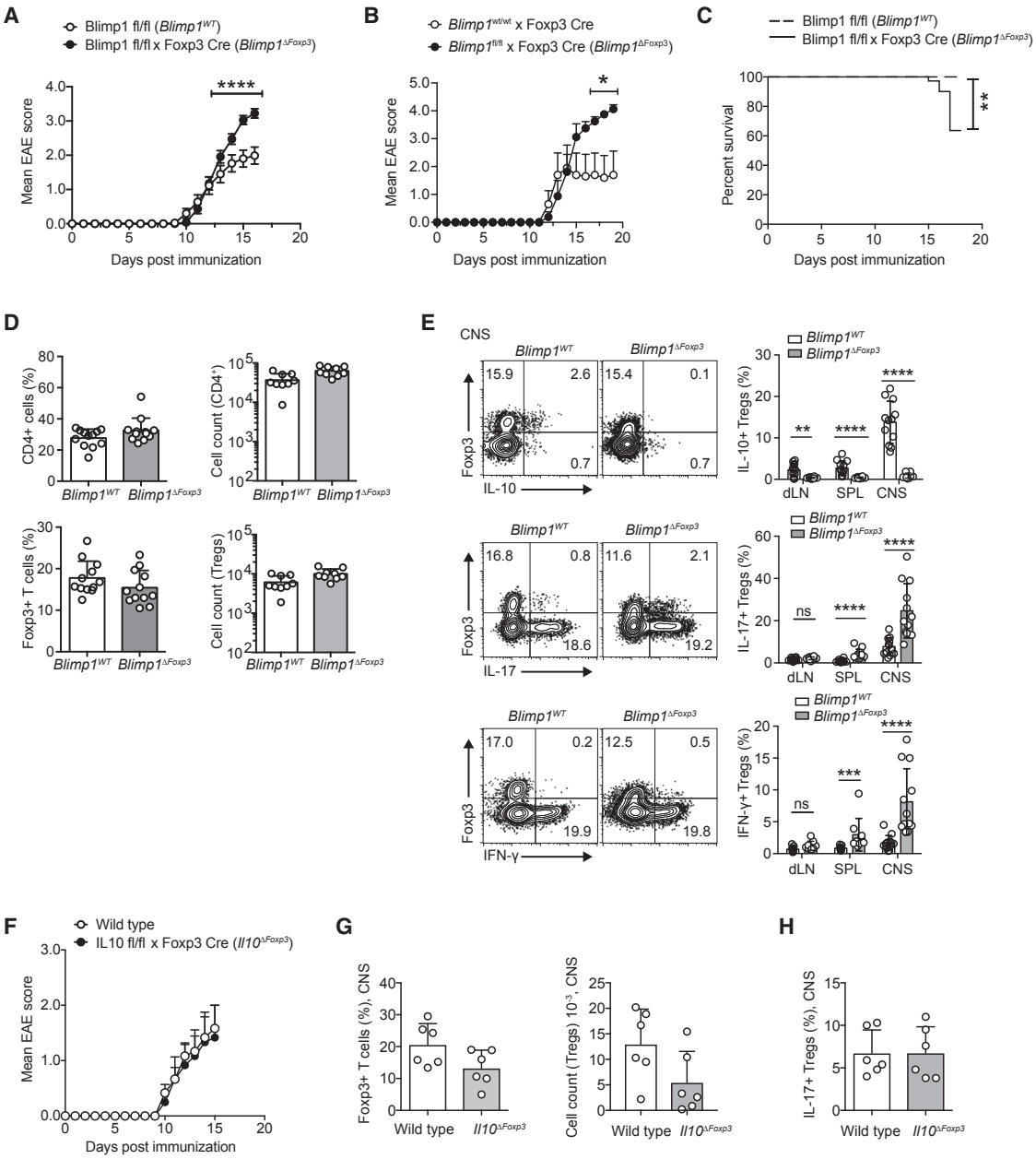

Figure 2. Ablation of Blimp1 in Treg Cells Results in Failure to Control CNS Inflammation

Blimp1$^{flox/flox}$ (*Blimp1*^{WT}) or *Foxp3 Cre* mice and *Blimp1*$^{flox/flox}$ × *Foxp3 Cre* (*Blimp1*$^{\Delta Foxp3}$) were immunized with MOG(35-55) in CFA to induce EAE. Mononuclear cells were isolated at the peak of EAE.

(A and B) EAE scores of *Blimp1*$^{\Delta Foxp3}$ mice in comparison to *Blimp1*^{WT} controls (A) and *Blimp1*$^{\Delta Foxp3}$ mice in comparison to *Cre* control mice (*Blimp1*$^{wt/wt}$ x *Foxp3 Cre*) (B). Data were summarized from three independent experiments. (*Blimp1*^{WT}, n = 20; *Foxp3 Cre*, n = 4; *Blimp1*$^{\Delta Foxp3}$, n = 31) (mean ± SEM). (two-way ANOVA, Sidak post test, $p < 0.05$).

(C) Survival curve. Data were summarized from three independent experiments (*Blimp1*^{WT}, n = 8; *Blimp1*$^{\Delta Foxp3}$, n = 10). Log-rank test (Mantel-Cox) (**$p < 0.01$).

(D) Frequencies and absolute cell numbers of live CD4$^+$ T cells and CD4$^+$Foxp3$^+$ Treg cells isolated from the CNS at the peak of EAE. Data were summarized from three independent experiments (mean ± SD).

(E) Mononuclear cells were isolated from the draining lymph node (dLN), spleen, and CNS and stimulated with PMA and ionomycin to analyze IL-10, IL-17, and IFN-γ in Treg cells by flow cytometry. Data are summarized from twelve biological replicates, derived from three independent experiments. Symbols depict individual mice (bars, mean ± SD). Mann-Whitney test (**$p < 0.01$; ***$p < 0.001$; ****$p < 0.0001$).

(F–H) Wild-type and *Il10*$^{flox/flox}$ × *Foxp3 Cre* (*Il10*$^{\Delta Foxp3}$) mice were immunized with MOG(35-55) in CFA to induce EAE. Wild-type, n = 6; *Il10*$^{\Delta Foxp3}$, n = 6 (mean ± SD) (F).

(legend continued on next page)

by the upregulation of inflammation sensing pathways, high expression of suppressive molecules, and the upregulation of Blimp1.

Blimp1 Is Maintained in CNS Treg Cells in a STAT1-Dependent Manner

TCR-induced IRF4 expression has been shown to drive Blimp1 expression in both Treg cells and conventional T cells (Cretney et al., 2011; Krishnamoorthy et al., 2017; Man et al., 2013). In addition, multiple cytokines in conjunction with TCR signaling have been shown to be able to induce Blimp1 expression through direct binding of signal transducer and activator of transcription (STAT) molecules to the *Prdm1* locus (Cretney et al., 2011; Heinemann et al., 2014; Kwon et al., 2009; Xin et al., 2016). Consistent with this notion, IL-10 and IL-21 (STAT3) and a number of inflammatory cytokines, including IFN-γ (STAT1), IL-12 (STAT4), and IL-27 (STAT3) induced Blimp1 in cultured splenic Treg cells (Figure 1H). To identify inflammatory pathways involved in Blimp1 expression in Treg cells during autoimmune CNS inflammation, we generated mixed bone marrow chimeric mice containing wild-type bone marrow together with either STAT1-deficient, STAT3-deficient (T cell-specific conditional using *Cd4 Cre*) or STAT4-deficient bone marrow. After induction of EAE, Treg cells were sorted from the CNS and spleens of these chimeric mice at the peak of EAE and assessed for expression of *Prdm1* (Blimp1) and its target *Il10*. When compared to the concomitant wild-type compartment, *Prdm1* was not reduced in STAT3-deficient and STAT4-deficient Treg cells (Figures S2A and S2B); however, it was markedly decreased in STAT1-deficient Treg cells (Figures 1I and 1J). Accordingly, the expression of *Il10* was lower in STAT1-deficient CNS Treg cells but not in STAT3- and STAT4-deficient Treg cells as compared to wild-type control Treg cells (Figures 1I, 1J, S2A and S2B). Consistent with these findings, *Il27r*$^{-/-}$ and *Il12rb2*$^{-/-}$ Treg cells isolated from mixed bone marrow chimeric mice showed unimpaired expression of *Il10* (Figure S2C and S2D). Thus, Blimp1 was induced in CNS Treg cells partially in a STAT1-dependent manner.

Blimp1 Is Indispensable for CNS Treg Cell Function

In order to test the function of Blimp1 in CNS Treg cells, we generated Treg cell conditional Blimp1-deficient mice (*Foxp3 Cre* x *Prdm1*$^{flox/flox}$, termed *Blimp1*$^{\Delta Foxp3}$). After immunization with MOG(35-55)+CFA, *Blimp1*$^{\Delta Foxp3}$ mice developed more severe signs of EAE as compared to both "floxed" control mice (*Prdm1*$^{flox/flox}$, termed *Blimp1*^{WT}) and "Cre" control mice (*Foxp3 Cre*), and a proportion succumbed to the disease (Figures 2A, 2B and 2C), indicating that Blimp1 expression in Foxp3^{+} Treg cells was mandatory for the control of CNS inflammation. Although the loss of Blimp1 in Treg cells did not affect the recruitment of Foxp3^{+} Treg cells to the CNS in *Blimp1*$^{\Delta Foxp3}$ mice (Figure 2D), *Blimp1*$^{\Delta Foxp3}$ Treg cells showed reduced expression of Foxp3, lost the expression of IL-10, and produced significantly more IL-17 and IFN-γ than their Blimp1-sufficient counterparts (Figure 2E).

Il10$^{-/-}$ mice develop more severe EAE (Bettelli et al., 1998), and we reasoned that the loss of Blimp1-dependent Treg cell effector functions, including IL-10 production, might be responsible for the failure of *Blimp1*$^{\Delta Foxp3}$ Treg cells to control CNS inflammation. However, Treg cell-specific ablation of *Il10* using *Il10*$^{\Delta Foxp3}$ (*Foxp3 Cre* × *Il10*$^{flox/flox}$) mice did not alter EAE disease severity or fraction and number of CNS Treg cells as compared to wild-type control mice (Figure 2F). Notably and in contrast to *Blimp1*$^{\Delta Foxp3}$ Treg cells, IL-10-deficient Treg cells isolated from the inflamed CNS did not exhibit a gain of IL-17 production as compared with their wild-type counterparts (Figures 2G and 2H). In summary, the loss of Blimp1 in Treg cells did not only result in a loss of distinct effector functions of Treg cells but appeared to lead to a more global loss of Treg cell identity in the inflamed CNS.

Blimp1 Controls Treg Cell Identity in the Inflamed CNS

In order to test whether Blimp1 controlled Treg cell identity in the inflamed CNS in a Treg cell-intrinsic manner, we generated mixed bone marrow chimeric mice by reconstituting Rag1-deficient recipient mice with a 1:1 mixture of congenically marked wild-type and *Blimp1*$^{\Delta Foxp3}$ bone marrow. At the peak of EAE, the CNS Treg cell compartment composed of wild-type (CD45.1) and *Blimp1*$^{\Delta Foxp3}$ (CD45.2) Treg cells was analyzed. *Blimp1*$^{\Delta Foxp3}$ CNS Treg cells showed a significant downregulation of Foxp3 as compared to their wild-type counterparts (Figure 3A). Furthermore, they had lost IL-10 expression and acquired IL-17 production (Figures 3B and 3C). RNA-seq and subsequent PCA of wild-type (WT) versus *Blimp1*$^{\Delta Foxp3}$ CNS Treg cells revealed that Blimp1-deficient Treg cells clustered consistently away from wild-type Treg cells, indicating Blimp1 regulated gene expression both in splenic and CNS Treg cells (Figure 3D). In total, we identified 342 genes upregulated (>2-fold, $p < 0.05$) and 409 genes downregulated (>2-fold, $p > 0.05$) in *Blimp1*$^{\Delta Foxp3}$ CNS Treg cells, including reduced expression of known Blimp1 target genes, such as *Il10* and *Gzmb* (Figure 3E; Table S2). Consistent with their increased production of IFN-γ, Blimp1-deficient CNS Treg cells expressed higher amounts of *Tbx21* (T-bet) (Figures S3A and S3B). In line with the reduced expression of Foxp3, genes normally suppressed by Foxp3 showed significant derepression in *Blimp1*$^{\Delta Foxp3}$ CNS Treg cells (Figure 3F). In summary, Blimp1 was required to maintain Foxp3 expression and a Treg cell-specific transcriptional profile in CNS Treg cells.

Blimp1 Controls Foxp3 in an Indirect Manner in Treg Cells

In order to address how Blimp1 controlled the transcriptional profile of CNS Treg cells, we performed assay for transposase-accessible chromatin using sequencing (ATAC-seq) in splenic and CNS Treg cells of mixed bone marrow chimeric mice

(G) Mononuclear cells were isolated from the CNS and analyzed for Foxp3 expression by flow cytometry. The graph represents the frequency and absolute cell numbers of Treg cells. Symbols depict individual mice (bars, mean ± SD).
(H) The isolated mononuclear cells from the CNS were stimulated with PMA and ionomycin to analyze IL-17 expression in Foxp3^{+} Treg cells by flow cytometry. Data are summarized from six biological replicates. Symbols depict individual mice (bars, mean ± SD).

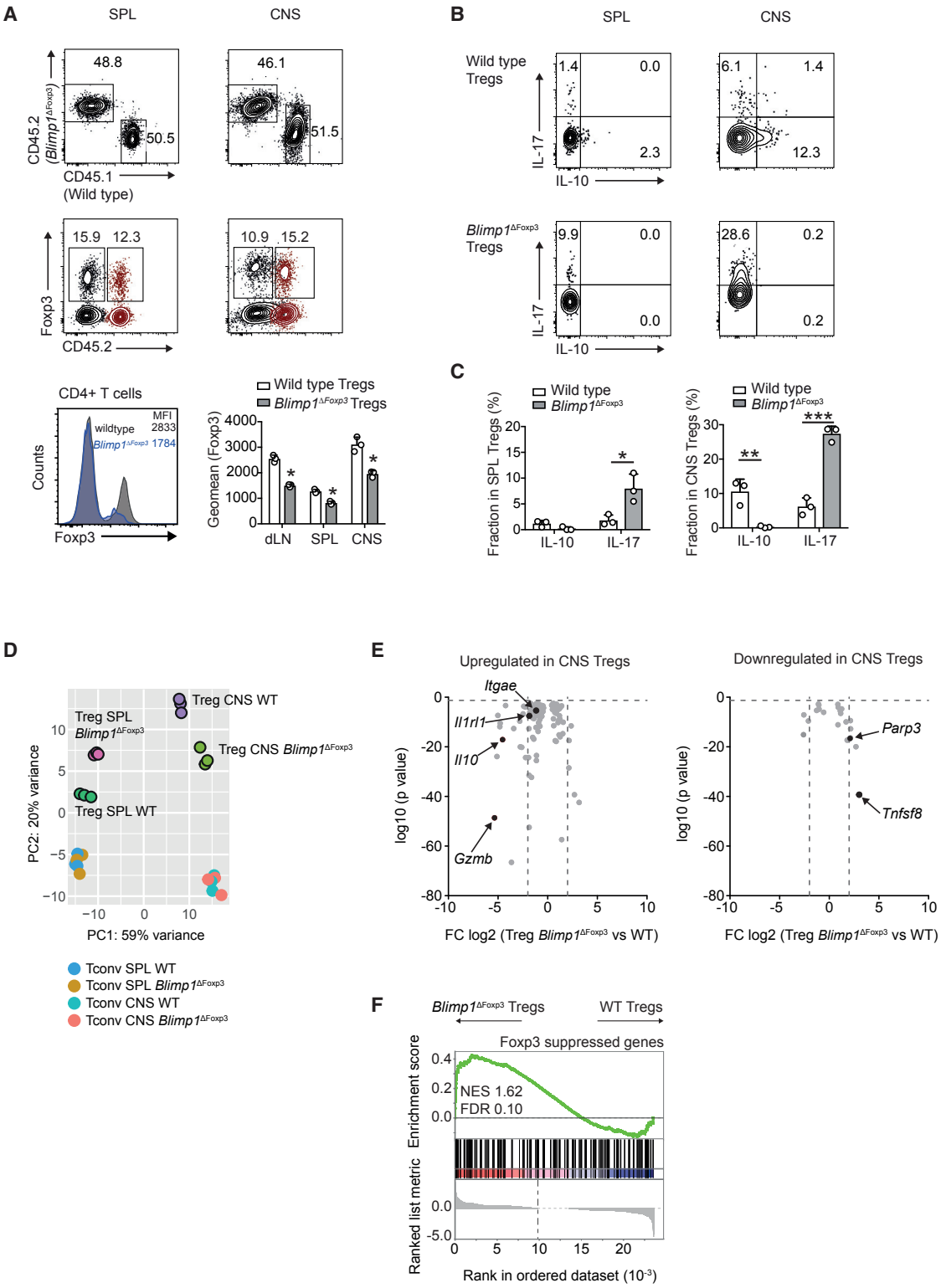

Figure 3. Blimp1 Governs Treg Cell Identity in CNS Treg Cells

Mixed bone marrow chimeras (MBMCs) were generated by reconstituting *Rag1*$^{-/-}$ hosts with (CD45.1, wild-type) and *Blimp1*$^{\Delta Foxp3}$ (CD45.2) bone marrow at a ratio of 1:1. The mixed bone marrow chimeras were immunized with MOG(35-55) in CFA to induce EAE. The mice were analyzed at the peak of EAE.

(legend continued on next page)

(wild-type plus *Blimp1*$^{\Delta Foxp3}$) at the peak of EAE. We then correlated the information about differentially accessible gene loci, including transcription factor-binding motifs with differences in gene expression between wild-type and *Blimp1*$^{\Delta Foxp3}$ CD4$^+$ T cells. In conventional T cells derived from the spleen of wild-type plus *Blimp1*$^{\Delta Foxp3}$ mixed bone marrow chimeras, no difference in ATAC peaks was detected as expected (Figure 4A). In splenic Treg cells, we identified 2,337 upregulated ATAC peaks in *Blimp1*$^{\Delta Foxp3}$ Treg cells, while 1,958 ATAC peaks were higher in wild-type Treg cells (Figure 4A). When we then interrogated these differential ATAC peaks for transcription factor-binding motifs, we identified a panel of transcription factors, including Ets, Runx1, and RORγt whose binding motifs were significantly enriched in splenic *Blimp1*$^{\Delta Foxp3}$ Treg cells as compared to wild-type Treg cells (Figures 4B and 4C). Conversely, motifs for nuclear factor κB (NF-κB) (p65), Erg, and AP1 transcription factors were prominent in ATAC peaks which were reduced in *Blimp1*$^{\Delta Foxp3}$ as compared to wild-type Treg cells (Figures 4B and 4C). Thus, the lack of Blimp1 prompted an altered transcriptional network to become operational in Foxp3$^+$ Treg cells under inflammatory conditions. Next, we asked to which extent Blimp1 was directly responsible for transcriptional changes in CNS Treg cells. Using a published Blimp1 chromatin immunoprecipitation sequencing (ChIP-seq) dataset (Mackay et al., 2016), we compared Blimp1 binding and ATAC peaks in the top 75 genes differentially expressed in *Blimp1*$^{\Delta Foxp3}$ versus wild-type CNS Treg cells. We identified 23 genes with Blimp1 binding sites within 50 kb of the promoter region, suggesting a direct role of Blimp1 in regulating their expression. Due to the different activity of Blimp1 as a repressor or promoter of transcription (Martins and Calame, 2008), we found that some of these genes were upregulated (e.g., *Crtam*), whereas others (such as *Il10*) were downregulated in *Blimp1*$^{\Delta Foxp3}$ CNS Treg cells as compared to wild-type CNS Treg cells (Figures 4D and 4E). In contrast, most of the top regulated genes did not show apparent Blimp1 binding despite changes in ATAC peaks, suggesting that their changed expression was not directly regulated by Blimp1. Importantly, in this category of genes, we observed reduced ATAC peaks within genes critical for Treg cell identity (such as the intron 1 enhancer of *Foxp3*) in *Blimp1*$^{\Delta Foxp3}$ versus wild-type CNS Treg cells (Figures 4D and 4E), suggesting that the regulation of Foxp3 in *Blimp1*$^{\Delta Foxp3}$ Treg cells was dependent on Blimp1 but likely not controlled by a direct transactivation activity of Blimp1 in the *Foxp3* locus.

Loss of Blimp1 Is Associated with Impaired Epigenetic Imprinting of the *Foxp3* Locus

Foxp3 expression is controlled by multiple mechanisms (Feng et al., 2014; Huehn et al., 2009). As we found no evidence for the direct control of the *Foxp3* locus by Blimp1, we explored the possibility of an epigenetic mechanism of Foxp3 regulation by Blimp1. Pyrosequencing analysis revealed a fully methylated CNS2 in conventional CD4$^+$ T cells derived from the CNS of *Blimp1*^{WT} plus *Blimp1*$^{\Delta Foxp3}$ mixed bone marrow chimeric mice as expected (Figure 5). In contrast, Foxp3$^+$ T cells were demethylated at CNS2, identifying them as bona fide Treg cells (Figure 5). However, both in the spleen and (in an even more pronounced manner) in the CNS, *Blimp1*$^{\Delta Foxp3}$ Treg cells showed a partial loss of the demethylated state of CNS2 as compared to wild-type Treg cells (Figure 5).

Because *Foxp3* was downregulated in Blimp1-deficient CNS Treg cells, it was possible that our analyses missed Treg cells that had substantially downregulated or lost Foxp3 (exTreg cells). We, therefore, performed a "fate-mapping" experiment by using an adoptive transfer approach. Bone marrow chimeric mice (wild-type [or *Foxp3 Cre* control] plus *Blimp1*$^{\Delta Foxp3}$) were immunized to increase the fraction of Blimp1-expressing Treg cells in the spleen, and the total Treg cell compartment from these donor mice comprising a mixture of wild-type (or *Foxp3 Cre* control) and *Blimp1*$^{\Delta Foxp3}$ Treg cells were transferred into recipient mice together with congenically marked (Thy1.1) conventional CD4$^+$ T cells (Figure 6A). After immunization with MOG(35-55) in CFA, Blimp1 sufficient control Treg cells and *Blimp1*$^{\Delta Foxp3}$ Treg cells were re-isolated from secondary hosts based on congenic markers (Figure 6B). Despite similar Ki67$^+$ fractions in wild-type and *Blimp1*$^{\Delta Foxp3}$ Treg cells (Figure 6C), the majority of *Blimp1*$^{\Delta Foxp3}$ Treg cells had lost Foxp3 expression, whereas wild-type Treg cells remained Foxp3 positive (Figure 6D). Accordingly, CNS2 as well as CpG islands of other key Treg cell loci, including the *Foxp3* promoter region and *Ctla4* in exTreg cells derived from *Blimp1*$^{\Delta Foxp3}$ Treg cells, were almost fully methylated (Figure 6E). In contrast, wild-type Treg cells kept the demethylated state of CNS2 in the *Foxp3* locus (Figure 6E).

Antagonistic Control of CNS2 (TSDR) Methylation by Blimp1 and IL-6-STAT3 through Dnmt3a

The methylation status of the *Foxp3* CNS2 has previously been shown to be controlled by the ten-eleven-translocation (Tet)

(A) Chimerism between wild-type and *Blimp1*$^{\Delta Foxp3}$ cells in the live CD4$^+$ gate of spleen and CNS mononuclear cells and analysis of Foxp3 expression by flow cytometry in control (wild-type) Treg cells and *Blimp1*$^{\Delta Foxp3}$ Treg cells isolated from the mixed bone marrow chimeras at the peak of EAE. Data are representative and summarized from three biological replicates. Symbols depict individual mice (bars, mean ± SD). Student's t test (*$p < 0.05$).
(B) Expression of IL-10 and IL-17 in Foxp3$^+$ Treg cells after *ex vivo* stimulation with PMA and ionomycin.
(C) Data were summarized from three biological replicates. Symbols depict individual mice (bars, mean ± SD). Student's t test (*$p < 0.05$).
(D–F) Treg cells and conventional CD4$^+$ T cells (Tconv) were sorted at the peak of EAE from the spleen and CNS of immunized mixed bone marrow chimeras (CD45.1 × *Foxp3*^{GFP}, wild-type; CD45.2, *Blimp1*$^{\Delta Foxp3}$ × *Foxp3*^{GFP}) and subjected to RNA-seq.
(D) Principal-component analysis of control Treg cells (wild-type), *Blimp1*$^{\Delta Foxp3}$ Treg cells, and Tconv cells isolated from mixed bone marrow chimeras, calculated for all genes with greatest difference according to gene expression, with $\log_2$ transformed row and column standardized data.
(E) Genes upregulated (top) or downregulated (bottom) in CNS Treg cells as compared to spleen Treg cells (see Figure 1) were assessed as to their expression in *Blimp1*$^{\Delta Foxp3}$ versus wild-type Treg cells and displayed in volcano plots.
(F) Enrichment of genes that are normally suppressed by Foxp3 (Williams and Rudensky, 2007) in *Blimp1*$^{\Delta Foxp3}$ CNS Treg cells as compared to wild-type Treg cells.
See also Figure S3 and Table S2.

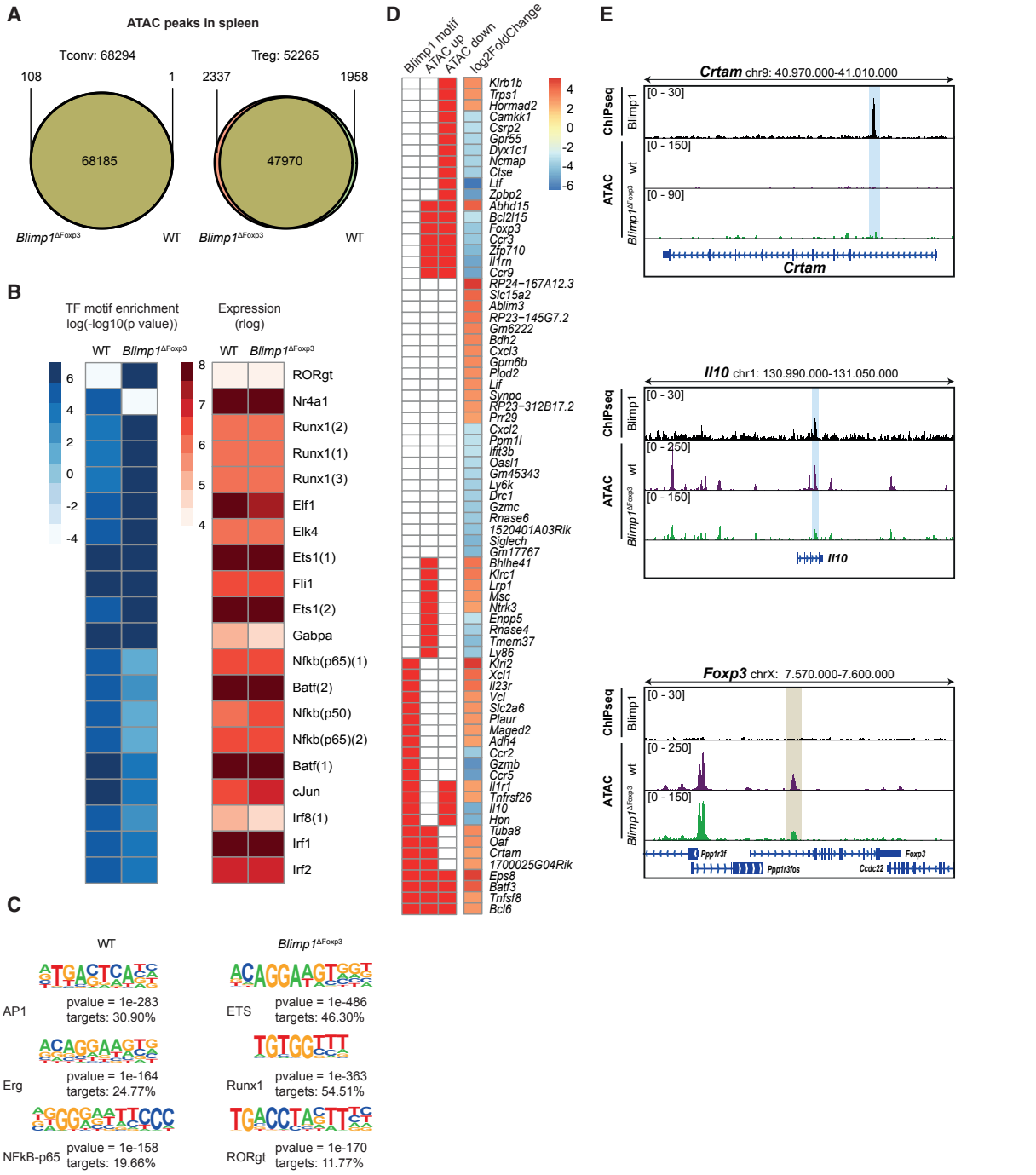

Figure 4. Blimp1 Regulates Genes in CNS Treg Cells in a Direct and Indirect Manner

(A) ATAC peaks in splenic wild-type and *Blimp1*$^{\Delta Foxp3}$ Tconv and Treg cells were quantified. Very few peaks were differentially enriched in Tconv cells (left), whereas substantial dysregulation could be identified in Treg cells (right).

(B) Transcription factor motif prediction in differential ATAC peaks of splenic wild-type versus *Blimp1*$^{\Delta Foxp3}$ Treg cells was performed with Homer by using known transcription factor motifs. Heatmap displays the log of the transcription factor (TF) prediction p value (left) and the expression of the respective transcription factors (right). For some transcription factors, multiple motifs were tested (denoted by numbers after the transcription factor name).

(C) Homer was used for *de novo* motif prediction in differential ATAC peaks of splenic wild-type versus *Blimp1*$^{\Delta Foxp3}$ Treg cells. The top 3 motifs of this analysis are shown.

(legend continued on next page)

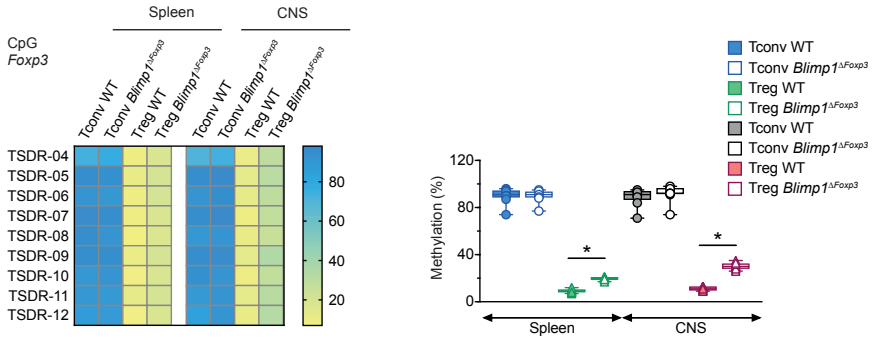

Figure 5. Blimp1 in Treg Cells Is Required to Maintain the Demethylated State of CNS2

Treg cells and Tconv cells from both the wild-type and *Blimp1*$^{\Delta Foxp3}$ compartments of mixed bone marrow chimeras were sorted from the spleen and the CNS according to experimental set up of Figure 3, and their genomic DNA was analyzed for the methylation status of CNS2 (TSDR). The data are representative of three independent biological replicates. Each line represents one CpG motif (left). The degree of methylation at each CpG motif is represented according to the color code. Cumulative quantification of the methylation of all CpG islands in CNS2 (TSDR) in Tconv and Treg cells as indicated (right). One-way ANOVA with Holm-Sidak's post-test (*$p < 0.0001$).

family of enzymes, which contribute to its demethylation (Yue et al., 2016), and DNA-methyltranferases (Dnmts), which oppose the activity of Tet enzymes and methylate CpG islands in the CNS2 (Feng et al., 2014; Josefowicz et al., 2009). Although genes encoding Tet molecules were not substantially de-regulated in *Blimp1*$^{\Delta Foxp3}$ Treg cells (Figure S4), we found significantly increased expression of *Dnmt3a* (but not *Dnmt1*) in Blimp1-deficient exTreg cells (Figure 6F). Notably, ATAC-seq analysis in CNS Treg cells isolated from mixed bone marrow chimeric mice at peak EAE showed an increase in ATAC peaks in *Dnmt3a* in *Blimp1*$^{\Delta Foxp3}$ CNS Treg cells as compared to wild-type CNS Treg cells, and re-analysis of Blimp1 ChIP-seq data (Mackay et al., 2016) confirmed Blimp1 binding in the *Dnmt3a* locus (Figure S4). In contrast, *Dnmt1* lacked ATAC peaks and Blimp1 binding in wild-type and *Blimp1*$^{\Delta Foxp3}$ CNS Treg cells, and the *Tet* loci either lacked or had decreased ATAC peaks in *Blimp1*$^{\Delta Foxp3}$ versus wild-type CNS Treg cells (Figure S4). Consistent with higher Dnmt3a expression in Blimp1-deficient versus control Treg cells, we found increased methylation of other known Dnmt3a target genes, including *Coro2a*, *Nfkbiz*, and *Ikzf3* (Kramer et al., 2017), in *Blimp1*$^{\Delta Foxp3}$ Treg cells re-isolated from MOG(35-55)+CFA-immunized secondary host mice compared to wild-type Treg cells (Figure 6G). Thus, our data indicated that in an inflammatory environment, *Dnmt3a* was suppressed by Blimp1.

Inflammatory signals have been associated with the loss of Treg cell identity (Zhou et al., 2009), and IL-6 in particular has been shown to drive the expression of inflammatory cytokines in Foxp3$^+$ Treg cells (Yang et al., 2008). We hypothesized that IL-6 may contribute to the loss of Foxp3 observed in *Blimp1*$^{\Delta Foxp3}$ Treg cells. Therefore, we interrogated the transcriptome of CNS Treg cells versus splenic Treg cells of EAE mice for the enrichment of IL-6 target genes. We found that IL-6 target genes were enriched in the transcriptome of CNS Treg cells as compared to splenic Treg cells (Figure 7A), suggesting that CNS Treg cells indeed sensed IL-6. We also hypothesized that IL-6 induced the expression of Dnmt3a, which would contribute to the methylation of the *Foxp3* locus. Notably, the *Dnmt3a* locus was more accessible in *Blimp1*$^{\Delta Foxp3}$ CNS Treg cells than in wild-type CNS Treg cells in our ATAC-seq analysis (Figure S4), and some genomic regions of *Dnmt3a* covered by ATAC peaks comprised STAT3 binding sites according to previously published STAT3 ChIP-seq data (Hirahara et al., 2015) in CD4$^+$ T cells (Figure S5A). In order to analyze the role of Blimp1 in the IL-6-mediated induction of Dnmt3a in wild-type Treg cells, we made use of the observation that KLRG1$^+$ Treg cells expressed high amounts of Blimp1, whereas KLRG1$^-$ Treg cells essentially lacked Blimp1 (Figure 7B) and tested the expression of Dnmt3 in KLRG1$^-$ Treg cells of wild-type and *Il6*$^{-/-}$ mice. Dnmt3a expression in sorted KLRG1$^-$ Foxp3 (GFP)$^+$ Treg cells in the spleen of *Il6*$^{-/-}$ mice was reduced as compared to wild-type littermates (Figure 7B), suggesting that IL-6 was required for the expression of Dnmt3a in KLRG1$^-$ Treg cells. Although the capacity to sense IL-6 was similar in Blimp1 (YFP)$^-$ and Blimp1 (YFP)$^+$ Treg cells (Figure S5B), IL-6 induced the downregulation of Foxp3 in Blimp1 (YFP)$^-$ but not Blimp1 (YFP)$^+$ Treg cells *in vitro* (Figure 7C). Interestingly, Blimp1 did not only bind directly to the *Dnmt3a* locus but also to the *Stat3* locus, where the binding of Blimp1 was associated with reduced ATAC peaks in wild-type as compared to *Blimp1*$^{\Delta Foxp3}$ Treg cells isolated from the CNS of mixed bone marrow chimeras (Figure S5A), consistent with the reduced expression of STAT3 in wild-type Treg cells as compared with *Blimp1*$^{\Delta Foxp3}$ Treg cells (see Figure S3B), indicating that Blimp1 might also suppress the expression of STAT3.

Finally, when KLRG1$^-$ Treg cells isolated from *Dnmt3a*$^{-/-}$ mice (*Dnmt3a*$^{flox/flox}$ x *Mx1 Cre*; *Dnmt3a*$^{\Delta Mx1}$) were exposed to IL-6 *in vitro*, the downregulation of Foxp3 was significantly less pronounced in *Dnmt3a*$^{-/-}$ Treg cells as compared to control

(D) Blimp1 peaks and differential ATAC peaks between wild-type and *Blimp1*$^{\Delta Foxp3}$ Treg cells in CNS were identified within 50 kb of the transcriptional start sites of differentially expressed genes. Heatmap displays Blimp1 binding and ATAC up- or downregulated peaks in the top 75 differentially expressed genes between wild-type and *Blimp1*$^{\Delta Foxp3}$ Treg cells in CNS (red bars).

(E) Intergrative genomics viewer (IGV) screenshots of Blimp1 ChIP-seq (Mackay et al., 2016) and ATAC-seq tracks for CNS wild-type and *Blimp1*$^{\Delta Foxp3}$ Treg cells. The scale of the *Blimp1*$^{\Delta Foxp3}$ Treg ATAC-seq track was adjusted to display comparable intensities for non-changed ATAC peaks due to the overall reduced signal intensity in this dataset.

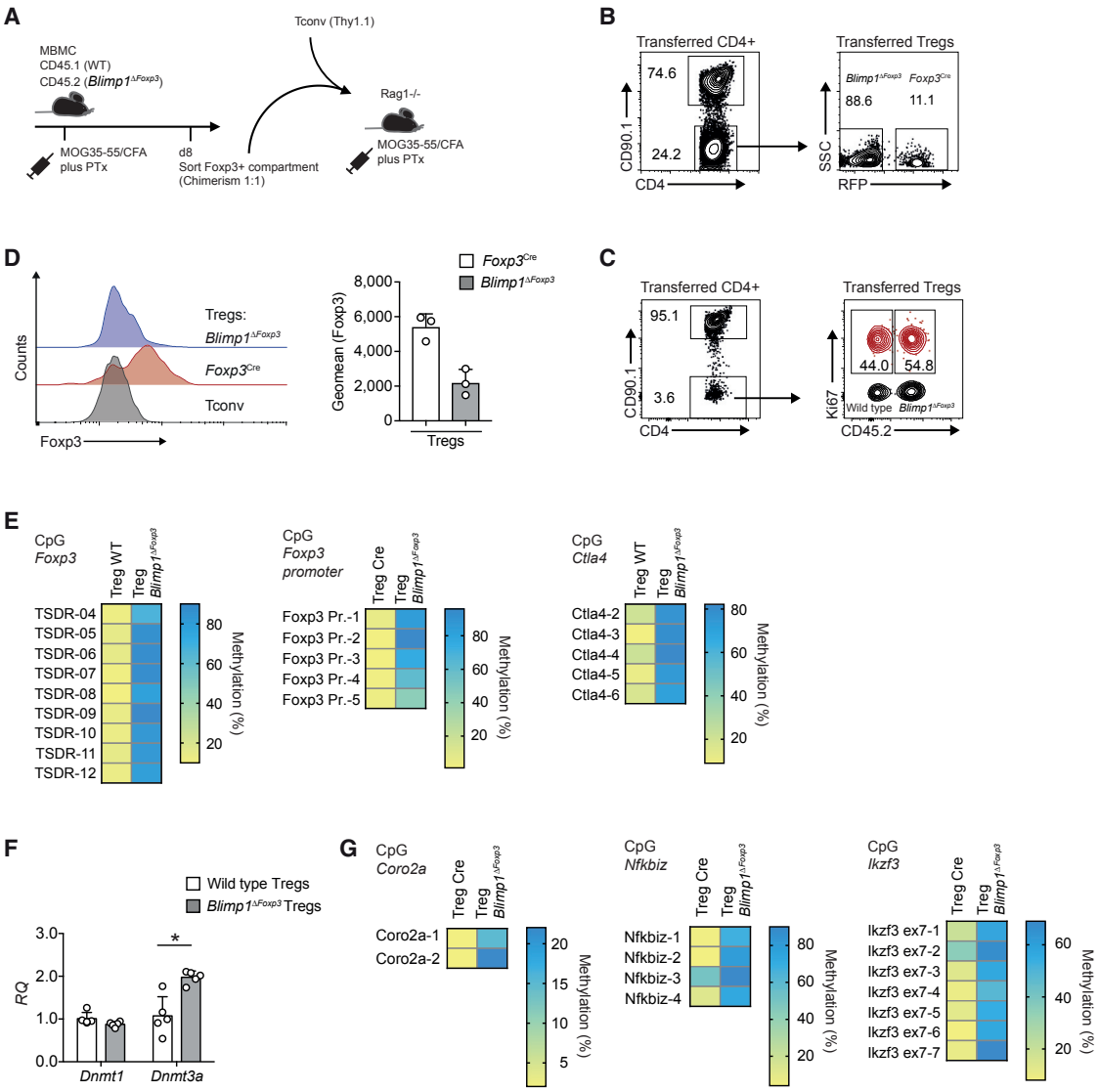

Figure 6. Lack of Blimp1 in Treg Cells Results in Instability of Treg Cells through Epigenetic Changes

(A) Schematic scheme of experimental set up.

(B and C) Total Treg cells, namely, both control Foxp3 Treg cells (*Foxp3 Cre*) (B) or wild-type (C) and *Blimp1*$^{\Delta Foxp3}$ Tre cells together, were sorted from spleen and draining lymph node of immunized mixed bone marrow chimeras on day 8 post-immunization and were transferred into *Rag1*$^{-/-}$ recipient mice along with congenically marked CD25^{-}CD44^{-}CD90.1^{+} naive conventional CD4^{+} T cells (Thy 1.1 Tconv). On day 1 post-transfer, the recipient mice were immunized with MOG(35-55) and CFA. Mononuclear cells were isolated from the spleen and draining lymph node for analysis 8 days post-immunization.

(C) Ki67 staining in wild-type and *Blimp1*$^{\Delta Foxp3}$ Treg cells re-isolated from the spleen of the secondary hosts. Representative of three independent biological replicates.

(D) Foxp3 expression was analyzed by intracellular staining. Frequency and geomean of Foxp3^{+} cells within the transferred *Foxp3 Cre* control Treg cells and *Blimp1*$^{\Delta Foxp3}$ Treg cells isolated from the spleen of secondary hosts. Cumulative data of five biological replicates derived from two independent experiments. Symbols depict individual mice (bars, mean ± SD). Student's t test (*$p < 0.05$).

(E) Wild-type and *Blimp1*$^{\Delta Foxp3}$ Treg cells were sorted from the secondary hosts, and genomic DNA was analyzed for methylation status of CNS2 (TSDR), *Foxp3* promoter, and *Ctla4*. Representative of three independent biological replicates. Each line represents one CpG motif. The degree of methylation at each CpG motif is depicted according to the color code.

(F) Gene expression of *Dnmt1* and *Dnmt3a* by qPCR in wild-type and *Blimp1*$^{\Delta Foxp3}$ Treg cells sorted from the spleen of secondary host mice. The expression of each gene was normalized to the control gene *Actb* and was plotted relative to the mean expression value of replicates for each gene. Cumulative data from five biological replicates, derived from two independent experiments. Symbols depict individual biological replicates (bars, mean ± SD). Student's t test (*$p < 0.05$).

(G) Methylation status of known Dnmt3a target genes in control Treg cells (*Foxp3 Cre* × *Blimp1*$^{wt/wt}$) and *Blimp1*$^{\Delta Foxp3}$ Treg cells (*Foxp3 Cre* × *Blimp1*$^{flox/flox}$) re-isolated from secondary hosts. Representative of three independent biological replicates. The degree of methylation at each CpG motif is depicted according to the color code.

See also Figure S4.

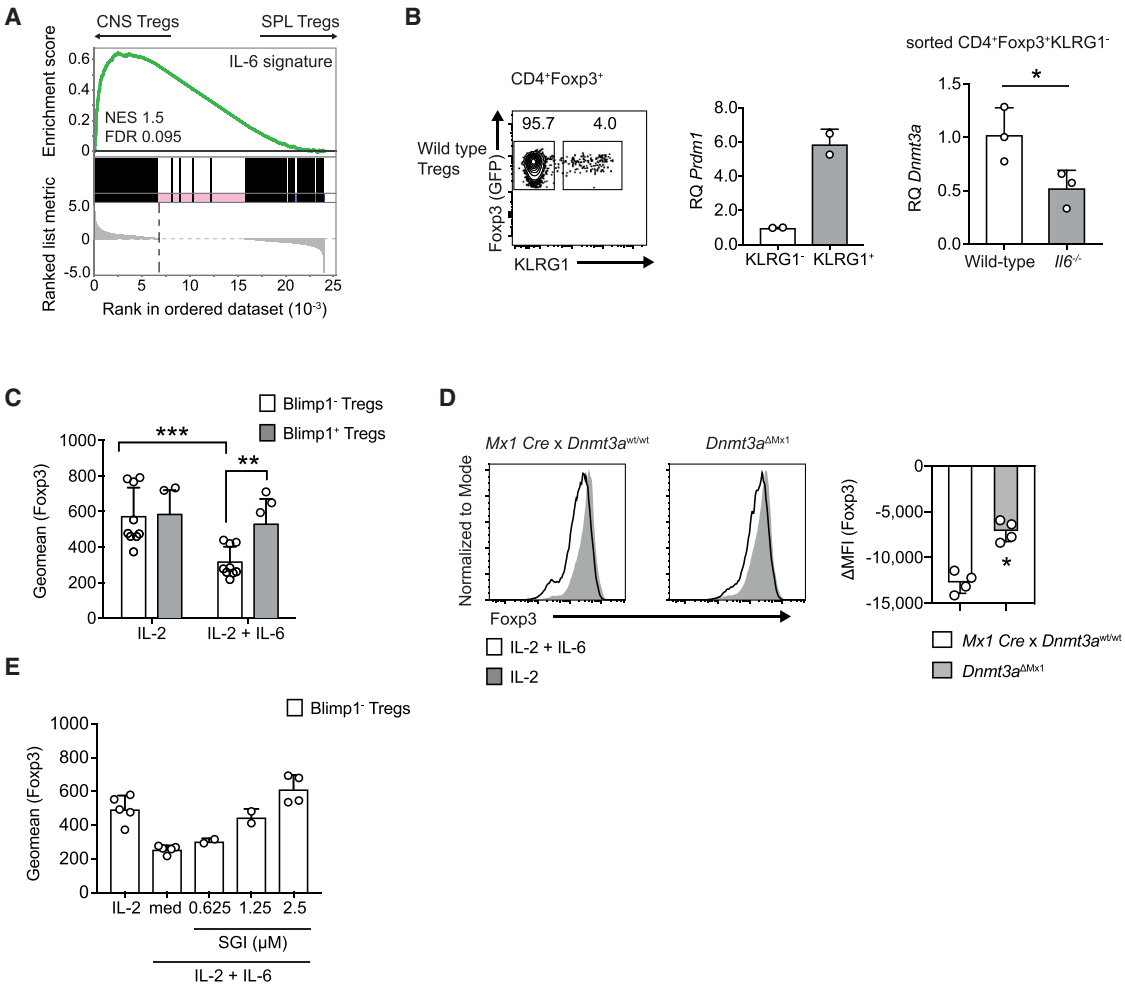

Figure 7. IL-6 Promotes the Loss of Foxp3 in Treg Cells in the Absence of Blimp1 by Inducing DNA Methylation

(A) Treg cells sense IL-6 in the inflamed CNS. The CNS Treg cell transcriptome (see Figure 1) is enriched for IL-6 signature genes as assessed by gene set enrichment analysis (GSEA).

(B) KLRG1$^-$Foxp3 (GFP)$^+$ and KLRG1$^+$Foxp3 (GFP)$^+$ Treg cells were sorted from spleen by flow cytometry of wild-type mice and tested for *Prdm1* (encoding Blimp1) expression by qPCR. Data are summarized from two biological replicates. KLRG1$^-$Blimp1$^-$Foxp3 (GFP)$^+$ Treg cells were sorted from spleen and lymph nodes of wild-type and *Il6*$^{-/-}$ mice and tested for *Dnmt3a* expression by qPCR. Data are summarized from three biological replicates. Symbols depict individual biological replicates (bars, mean ± SD). Student's t test (*$p < 0.05$).

(C) Blimp1 (YFP) $^-$ and Blimp1 (YFP)$^+$ Treg cells were sorted from the spleen and LNs of unmanipulated Blimp1 (YFP) reporter mice and stimulated with anti-CD3 and anti-CD28 dynabeads in the presence of either IL-2 alone or IL-2 and IL-6. On day 4, cultured Treg cells were analyzed for Foxp3 expression by intracellular staining. Cumulative data of three independent experiments, (mean ± SD). Two-way ANOVA (Sidak's multiple comparison test), $p < 0.05$.

(D) Lack of Dnmt3a reduces loss of Foxp3 in Treg cells in response to IL-6. KLRG1$^-$ (Blimp1$^-$) Foxp3$^+$ Treg cells were purified from the spleen and LNs of control mice or inducible Dnmt3a-deficient animals (*Dnmt3a*$^{\Delta Mx1}$), cultured in the absence or presence of IL-6, and assessed for Foxp3 expression by flow cytometry after 4 days. Representative histograms of Foxp3 expression in IL-2 alone or IL-2 and IL-6 cultured control or *Dnmt3a*$^{\Delta Mx1}$ Treg cells. ΔMFI (mean fluorescence intensity; Foxp3) in individual mice (bars, mean ± SD). Student's t test (*$p < 0.05$).

(E) In some cultures, the Blimp1 (YFP)$^-$ Treg cells were additionally treated with SGI-1027 at indicated concentrations to block Dnmt3a activity and analyzed for Foxp3 expression level on day 5 of culture. Cumulative data from two independent experiments.

See also Figure S5.

Treg cells (*Dnmt3a*$^{wt/wt}$ × *Mx1 Cre*) (Figure 7D). In addition, the IL-6-induced loss of Foxp3 in Blimp1$^-$ Treg cells was rescued when Dnmt3a was pharmacologically blocked using the inhibitor SGI-1027 (Figures 7E and S5C). Thus, the loss of Dnmt3a by genetic ablation or pharmacologic inhibition protected Blimp1$^-$ Treg cells from the loss of Foxp3. In summary, our data indicated that Blimp1 controlled the stability of Treg cells by suppressing the expression and function of Dnmt3a, which was induced in an inflammatory environment in an IL-6-STAT3-dependent manner.

DISCUSSION

Treg cells have been shown to be remarkably stable and can preserve their identity and function in a range of conditions both during steady state and in inflammation (Rubtsov et al., 2010). A variety of signals, including costimulatory signals, were identified to contribute to the stability of Treg cells (DuPage et al., 2015). However, Treg cells lose their identity upon the loss of Foxp3 expression (Williams and Rudensky, 2007), and the idea of lineage stability of Treg cells has been challenged in severe inflammation (Zhou et al., 2009). On the other hand, proinflammatory cytokines, including IL-12, IL-27, and IFN-γ, have been shown to shape Treg cell responses. Although IL-12 and IL-27 are considered to adapt Treg cells to suppress the corresponding (Th1) effector responses (Hall et al., 2012; Koch et al., 2009), IFN-γ has been reported to induce an intrinsic "fragility of Treg cells," even though it does not induce a loss of Foxp3 (Overacre-Delgoffe et al., 2017). Yet, sensing of IFN-γ by Treg cells is also important for their IL-10 production in the context of Th1 responses (Koch et al., 2012). This is consistent with our data, which show that STAT1 signaling in Treg cells is required for the expression of Blimp1, a major regulator of IL-10 in Treg cells (Cretney et al., 2011), and is a factor required to maintain Foxp3 expression as we show here. Although STAT3, STAT4, and STAT5 regulate Blimp1 expression in conventional T cells (Heinemann et al., 2014; Kwon et al., 2009; Neumann et al., 2014; Xin et al., 2016), STAT1 has been shown to directly transactivate the promoter of *Blimp1* in B cells (Chen et al., 2016). Whether STAT1 activation in Treg cells is dependent on the canonical interferon-induced pathway or non-canonical STAT1 activation by TLR signals (Luu et al., 2014) remains to be determined. Notably, although IL-10 derived from conventional T cells is required to induce full suppressive effector functions in Treg cells (Chaudhry et al., 2011; Heinemann et al., 2014), genetic ablation of the IL-10 receptor (*Il10ra*) in Treg cells is not associated with a loss of Foxp3 expression (Chaudhry et al., 2011). Therefore, our data support the idea that proinflammatory (rather than anti-inflammatory) cytokine signals appear to initiate a feedback loop that maintains Treg cell identity and function in an inflammatory environment.

Blimp1-mediated maintenance of Treg cell stability becomes indispensable under "inflammatory pressure." Interestingly, it has previously been reported in a fate mapping system that a subset of Foxp3$^+$ Treg cells loses Foxp3 expression and becomes proinflammatory (Bailey-Bucktrout et al., 2013), and it is intriguing to speculate that these are Foxp3$^+$ Treg cells that fail to sufficiently upregulate Blimp1. In fact, in two recently published studies, lower expression of Foxp3 in Blimp1-deficient Treg cells was measured but not further explored (Bankoti et al., 2017; Ogawa et al., 2018). Yet, a stronger proliferation of Blimp1-deficient as compared to Blimp1-sufficient Treg cells was observed, which is consistent with lower levels of Foxp3 in Blimp-deficient Treg cells (Bankoti et al., 2017). Here, our data provide a mechanistic underpinning for cytokine-guided stability or plasticity of Treg cells by linking cytokine signaling pathways to the Blimp1-mediated transcriptional modulation of the enzymatic machinery that controls DNA methylation in *cis* regulatory elements of the *Foxp3* locus. Tet family enzymes and Dnmts are opposing players in demethylating or methylating CpG islands within DNA elements in immune cells and non-immune cells (Tang et al., 2015). Unmethylated DNA is *de novo* methylated by Dnmt3a, whereas Dnmt1 is responsible for the maintenance of pre-existing methylation (Lyko, 2018). Consistent with this model, under conditions of inflammation, Dnmt3a might be more important for the *de novo* methylation of the usually fully demethylated CNS2 of Treg cells. We observed an upregulation of Dnmt3a in Blimp1-deficient Treg cells. Together with a guided recruitment of Dnmt3a to DNA sites (Hervouet et al., 2009) perhaps facilitated by transcription factors such as Ets1, which binds to CNS2 (Polansky et al., 2010) and whose binding motif is overrepresented in the ATAC peaks of *Blimp1*$^{\Delta Foxp3}$ Treg cells, Dnmt3a might not only be more abundant but also more active in *Blimp1*$^{\Delta Foxp3}$ Treg cells as compared to wild-type Treg cells, resulting in methylation of distinct target loci.

In Treg cells, CNS2 acts as a sensor for IL-2 whose downstream signal transducer STAT5 binds to CNS2. The susceptibility of this sensor to STAT5 binding is, in turn, controlled by its methylation status (Feng et al., 2014). IL-6-STAT3-mediated Dnmt3a activation promotes CNS2 methylation and, thus, likely abrogates STAT5 binding, resulting in reduced Foxp3 transcription under limiting IL-2 conditions (Feng et al., 2014). Our data suggest that there might be a direct antagonistic control of *Dnmt3a* by STAT3 versus Blimp1 (see Figure S5D). Our model is not mutually exclusive with the idea that some genes that are suppressed by Foxp3 (Zhou et al., 2008) are also directly (transcriptionally) suppressed by Blimp1. For instance, direct suppression of *Il17a* has recently been described in Helios$^-$RORγt$^+$ pTregs in the intestine (Ogawa et al., 2018). However, in autoimmune CNS inflammation, pTreg cells are not induced (Josefowicz et al., 2012; Korn et al., 2007), and the "toxic gain" of IL-17 production, which we observed in Blimp1-deficient CNS Treg cells, only represents a minor contribution to the overall production of IL-17 in the CNS of EAE mice. Therefore, we conclude that the global loss of Treg cell identity through the loss of Foxp3 expression as a consequence of a lack of Blimp1 in CNS Treg cells is responsible for the uncontrolled inflammatory phenotype that we noticed in *Blimp1*$^{\Delta Foxp3}$ mice. In future studies, it will have to be seen how the Blimp1-mediated transcriptional regulation of Dnmt3a and its recruitment to DNA loci determine a hierarchy of epigenetic regulation of distinct genetic loci in Treg cells. In addition, the activation of the IL-6-STAT3 pathway has many downstream targets, and specific modulators of that pathway that result in enhanced expression and function of Dnmt3a in Treg cells need to be identified.

In summary, we have identified a mechanism that antagonizes IL-6-STAT3-induced abrogation of Foxp3 in tTreg cells. This pathway is Blimp1 dependent and supports Treg cell identity at sites of inflammation by keeping CNS2 in a demethylated state, thus allowing the continuous expression of Foxp3 and maintenance of suppressive function. The opposing activities of STAT3 and Blimp1 converging on Dnmt3a will be interesting to further explore for druggable targets that could be used to stabilize Treg cells in autoimmunity and destabilize them for the treatment of cancer.

STAR★METHODS

Detailed methods are provided in the online version of this paper and include the following:

- KEY RESOURCES TABLE
- CONTACT FOR REAGENT AND RESOURCE SHARING
- EXPERIMENTAL MODELS AND SUBJECT DETAILS
  - Animals
- METHOD DETAILS
  - Generation of mixed bone marrow chimeras
  - Induction of EAE
  - Adoptive transfer of Treg cells
  - Preparation of mononuclear cells from the central nervous system (CNS)
  - Preparation of peripheral T cells
  - Cell culture
  - Antibodies and flow cytometry
  - Quantitative PCR
  - RNA-seq
  - ChIP-seq
  - ATAC-seq
  - Methylation analysis
- QUANTIFICATION AND STATISTICAL ANALYSIS
- DATA AVAILABILITY

SUPPLEMENTAL INFORMATION

Supplemental Information includes five figures and two tables and can be found with this article online at https://doi.org/10.1016/j.celrep.2019.01.070.

ACKNOWLEDGMENTS

We would like to thank Veronika Husterer for her skillful technical assistance. We thank Beate Pietzsch for performing bisulfite pyrosequencing. We would also like to thank Veronika Holecska and Max Löhning (DRFZ Berlin) for providing us the isolated bones of *Stat4*$^{-/-}$ mice. We are grateful to Mohammad Oukka (University of Washington, Seattle, USA), Veit Buchholz (Technical University of Munich), and Stephan Kemmner (Technical University of Munich) for providing mouse strains. This work was supported by the Deutsche Forschungsgemeinschaft (SFB1054-B06 to T.K., TRR128 to T.K. and A.W., SyNergy to T.K., SFB738-C07 to J.H., SFB1243-A03 to G.S., and SFB1321-project number 329628492 to G.S.), the German Ministry of Education and Research (BMBF, T-B in NMO), the Helmholtz Gemeinschaft (Zukunftsthema "Immunology and Inflammation," ZT-0027 to J.H.), the ERC (CoG 647215 to T.K.), project grants from the National Health and Medical Research Council (1069075 and 1106378 to A.K.), a fellowship from the Sylvia and Charles Viertel foundation (to A.K.), and the National Multiple Sclerosis Society (NMSS RG 1707-28780 to A.W.). This study was also supported through Victorian State Government Operational Infrastructure Support and Australian Government NHMRC Independent Research Institute Infrastructure Support scheme.

AUTHOR CONTRIBUTIONS

G.G. designed and performed most experiments and drafted the manuscript. A.M., A.V., Y.Z., T.R., M.H., C.P., L.A., and B.K. performed or contributed to specific experiments. G.L. performed RNA-seq data analysis. H.M. and G.S. generated and analyzed ATAC-seq data. S.F. and J.H. performed bisulfite pyrosequencing and interpreted the methylation data. R.O. and R.R. generated RNA-seq data. L.P., R.K., and M.K. provided reagents and analyzed data. A.W. supervised and analyzed EAE (*Foxp3 Cre*) data. A.K. supervised experiments, analyzed data, and edited the manuscript. T.K. conceptualized the study, supervised the experiments, analyzed data, and wrote the manuscript.

DECLARATION OF INTERESTS

The authors declare no competing financial interests.

Received: February 8, 2018
Revised: December 13, 2018
Accepted: January 17, 2019
Published February 12, 2019

REFERENCES

Abbas, A.K., Benoist, C., Bluestone, J.A., Campbell, D.J., Ghosh, S., Hori, S., Jiang, S., Kuchroo, V.K., Mathis, D., Roncarolo, M.G., et al. (2013). Regulatory T cells: recommendations to simplify the nomenclature. Nat. Immunol. *14*, 307–308.

Agarwal, P., Raghavan, A., Nandiwada, S.L., Curtsinger, J.M., Bohjanen, P.R., Mueller, D.L., and Mescher, M.F. (2009). Gene regulation and chromatin remodeling by IL-12 and type I IFN in programming for CD8 T cell effector function and memory. J. Immunol. *183*, 1695–1704.

Bailey-Bucktrout, S.L., Martínez-Llordella, M., Zhou, X., Anthony, B., Rosenthal, W., Luche, H., Fehling, H.J., and Bluestone, J.A. (2013). Self-antigen-driven activation induces instability of regulatory T cells during an inflammatory autoimmune response. Immunity *39*, 949–962.

Bankoti, R., Ogawa, C., Nguyen, T., Emadi, L., Couse, M., Salehi, S., Fan, X., Dhall, D., Wang, Y., Brown, J., et al. (2017). Differential regulation of effector and fegulatory T cell function by Blimp1. Sci. Rep. *7*, 12078.

Bettelli, E., Das, M.P., Howard, E.D., Weiner, H.L., Sobel, R.A., and Kuchroo, V.K. (1998). IL-10 is critical in the regulation of autoimmune encephalomyelitis as demonstrated by studies of IL-10- and IL-4-deficient and transgenic mice. J. Immunol. *161*, 3299–3306.

Buenrostro, J.D., Giresi, P.G., Zaba, L.C., Chang, H.Y., and Greenleaf, W.J. (2013). Transposition of native chromatin for fast and sensitive epigenomic profiling of open chromatin, DNA-binding proteins and nucleosome position. Nat, Methods *10*, 1213–1218.

Chaudhry, A., Samstein, R.M., Treuting, P., Liang, Y., Pils, M.C., Heinrich, J.-M., Jack, R.S., Wunderlich, F.T., Brüning, J.C., Müller, W., and Rudensky, A.Y. (2011). Interleukin-10 signaling in regulatory T cells is required for suppression of Th17 cell-mediated inflammation. Immunity *34*, 566–578.

Chen, T.-T., Tsai, M.-H., Kung, J.T., Lin, K.-I., Decker, T., and Lee, C.-K. (2016). STAT1 regulates marginal zone B cell differentiation in response to inflammation and infection with blood-borne bacteria. J. Exp. Med. *213*, 3025–3039.

Choi, Y.S., Kageyama, R., Eto, D., Escobar, T.C., Johnston, R.J., Monticelli, L., Lao, C., and Crotty, S. (2011). ICOS receptor instructs T follicular helper cell versus effector cell differentiation via induction of the transcriptional repressor Bcl6. Immunity *34*, 932–946.

Corces, M.R., Trevino, A.E., Hamilton, E.G., Greenside, P.G., Sinnott-Armstrong, N.A., Vesuna, S., Satpathy, A.T., Rubin, A.J., Montine, K.S., Wu, B., et al. (2017). An improved ATAC-seq protocol reduces background and enables interrogation of frozen tissues. Nat. Methods *14*, 959–962.

Cretney, E., Xin, A., Shi, W., Minnich, M., Masson, F., Miasari, M., Belz, G.T., Smyth, G.K., Busslinger, M., Nutt, S.L., and Kallies, A. (2011). The transcription factors Blimp-1 and IRF4 jointly control the differentiation and function of effector regulatory T cells. Nat. Immunol. *12*, 304–311.

DuPage, M., Chopra, G., Quiros, J., Rosenthal, W.L., Morar, M.M., Holohan, D., Zhang, R., Turka, L., Marson, A., and Bluestone, J.A. (2015). The chromatin-modifying enzyme Ezh2 is critical for the maintenance of regulatory T cell identity after activation. Immunity *42*, 227–238.

Durbin, J.E., Hackenmiller, R., Simon, M.C., and Levy, D.E. (1996). Targeted disruption of the mouse Stat1 gene results in compromised innate immunity to viral disease. Cell *84*, 443–450.

Feng, Y., Arvey, A., Chinen, T., van der Veeken, J., Gasteiger, G., and Rudensky, A.Y. (2014). Control of the inheritance of regulatory T cell identity by a cis element in the Foxp3 locus. Cell *158*, 749–763.

Floess, S., Freyer, J., Siewert, C., Baron, U., Olek, S., Polansky, J., Schlawe, K., Chang, H.-D., Bopp, T., Schmitt, E., et al. (2007). Epigenetic control of the foxp3 locus in regulatory T cells. PLoS Biol. *5*, e38.

Hall, A.O., Beiting, D.P., Tato, C., John, B., Oldenhove, G., Lombana, C.G., Pritchard, G.H., Silver, J.S., Bouladoux, N., Stumhofer, J.S., et al. (2012). The cytokines interleukin 27 and interferon-γ promote distinct Treg cell populations required to limit infection-induced pathology. Immunity *37*, 511–523.

Heinemann, C., Heink, S., Petermann, F., Vasanthakumar, A., Rothhammer, V., Doorduijn, E., Mitsdoerffer, M., Sie, C., Prazeres da Costa, O., Buch, T., et al. (2014). IL-27 and IL-12 oppose pro-inflammatory IL-23 in CD4+ T cells by inducing Blimp1. Nat. Commun. *5*, 3770.

Heinz, S., Benner, C., Spann, N., Bertolino, E., Lin, Y.C., Laslo, P., Cheng, J.X., Murre, C., Singh, H., and Glass, C.K (2010). Simple combinations of lineage-determining transcription factors prime cis-regulatory elements required for macrophage and B cell identities. Mol. Cell. *38*, 576–589.

Hervouet, E., Vallette, F.M., and Cartron, P.-F. (2009). Dnmt3/transcription factor interactions as crucial players in targeted DNA methylation. Epigenetics *4*, 487–499.

Hirahara, K., Onodera, A., Villarino, A.V., Bonelli, M., Sciumè, G., Laurence, A., Sun, H.-W., Brooks, S.R., Vahedi, G., Shih, H.-Y., et al. (2015). Asymmetric action of STAT transcription factors drives transcriptional outputs and cytokine specificity. Immunity *42*, 877–889.

Huehn, J., Polansky, J.K., and Hamann, A. (2009). Epigenetic control of FOXP3 expression: the key to a stable regulatory T-cell lineage? Nat. Rev. Immunol. *9*, 83–89.

Josefowicz, S.Z., Wilson, C.B., and Rudensky, A.Y. (2009). Cutting edge: TCR stimulation is sufficient for induction of Foxp3 expression in the absence of DNA methyltransferase 1. J. Immunol. *182*, 6648–6652.

Josefowicz, S.Z., Niec, R.E., Kim, H.Y., Treuting, P., Chinen, T., Zheng, Y., Umetsu, D.T., and Rudensky, A.Y. (2012). Extrathymically generated regulatory T cells control mucosal TH2 inflammation. Nature *482*, 395–399.

Kallies, A., Xin, A., Belz, G.T., and Nutt, S.L. (2009). Blimp-1 transcription factor is required for the differentiation of effector CD8(+) T cells and memory responses. Immunity *31*, 283–295.

Kaplan, M.H., Sun, Y.L., Hoey, T., and Grusby, M.J. (1996). Impaired IL-12 responses and enhanced development of Th2 cells in Stat4-deficient mice. Nature *382*, 174–177.

Kim, B.-S., Lu, H., Ichiyama, K., Chen, X., Zhang, Y.-B., Mistry, N.A., Tanaka, K., Lee, Y.-H., Nurieva, R., Zhang, L., et al. (2017). Generation of RORγt^{+} antigen-specific T regulatory 17 cells from Foxp3^{+} precursors in autoimmunity. Cell Rep. *21*, 195–207.

Koch, M.A., Tucker-Heard, G., Perdue, N.R., Killebrew, J.R., Urdahl, K.B., and Campbell, D.J. (2009). The transcription factor T-bet controls regulatory T cell homeostasis and function during type 1 inflammation. Nat. Immunol. *10*, 595–602.

Koch, M.A., Thomas, K.R., Perdue, N.R., Smigiel, K.S., Srivastava, S., and Campbell, D.J. (2012). T-bet(+) Treg cells undergo abortive Th1 cell differentiation due to impaired expression of IL-12 receptor β2. Immunity *37*, 501–510.

Kopf, M., Baumann, H., Freer, G., Freudenberg, M., Lamers, M., Kishimoto, T., Zinkernagel, R., Bluethmann, H., and Köhler, G. (1994). Impaired immune and acute-phase responses in interleukin-6-deficient mice. Nature *368*, 339–342.

Korn, T., Reddy, J., Gao, W., Bettelli, E., Awasthi, A., Petersen, T.R., Bäckström, B.T., Sobel, R.A., Wucherpfennig, K.W., Strom, T.B., et al. (2007). Myelin-specific regulatory T cells accumulate in the CNS but fail to control autoimmune inflammation. Nat. Med. *13*, 423–431.

Korn, T., Mitsdoerffer, M., Croxford, A.L., Awasthi, A., Dardalhon, V.A., Galileos, G., Vollmar, P., Stritesky, G.L., Kaplan, M.H., Waisman, A., et al. (2008). IL-6 controls Th17 immunity in vivo by inhibiting the conversion of conventional T cells into Foxp3+ regulatory T cells. Proc. Natl. Acad. Sci. USA *105*, 18460–18465.

Kramer, A.C., Kothari, A., Wilson, W.C., Celik, H., Nikitas, J., Mallaney, C., Ostrander, E.L., Eultgen, E., Martens, A., Valentine, M.C., et al. (2017). Dnmt3a regulates T-cell development and suppresses T-ALL transformation. Leukemia *31*, 2479–2490.

Krishnamoorthy, V., Kannanganat, S., Maienschein-Cline, M., Cook, S.L., Chen, J., Bahroos, N., Sievert, E., Corse, E., Chong, A., and Sciammas, R. (2017). The IRF4 gene regulatory module functions as a read-write integrator to dynamically coordinate T helper cell fate. Immunity *47*, 481–497.e7.

Kwon, H., Thierry-Mieg, D., Thierry-Mieg, J., Kim, H.-P., Oh, J., Tunyaplin, C., Carotta, S., Donovan, C.E., Goldman, M.L., Tailor, P., et al. (2009). Analysis of interleukin-21-induced Prdm1 gene regulation reveals functional cooperation of STAT3 and IRF4 transcription factors. Immunity *31*, 941–952.

Lahl, K., Loddenkemper, C., Drouin, C., Freyer, J., Arnason, J., Eberl, G., Hamann, A., Wagner, H., Huehn, J., and Sparwasser, T. (2007). Selective depletion of Foxp3+ regulatory T cells induces a scurfy-like disease. J. Exp. Med. *204*, 57–63.

Langmead, B. (2010). Aligning short sequencing reads with Bowtie. Curr. Protoc. Bioinformatics *Chapter 11*, Unit 11.17.

Lee, P.P., Fitzpatrick, D.R., Beard, C., Jessup, H.K., Lehar, S., Makar, K.W., Pérez-Melgosa, M., Sweetser, M.T., Schlissel, M.S., Nguyen, S., et al. (2001). A critical role for Dnmt1 and DNA methylation in T cell development, function, and survival. Immunity *15*, 763–774.

Love, M.I., Huber, W., and Anders, S. (2014). Moderated estimation of fold change and dispersion for RNA-seq data with DESeq2. Genome Biol. *15*, 550.

Luche, H., Weber, O., Nageswara Rao, T., Blum, C., and Fehling, H.J. (2007). Faithful activation of an extra-bright red fluorescent protein in "knock-in" Cre-reporter mice ideally suited for lineage tracing studies. Eur. J. Immunol. *37*, 43–53.

Luu, K., Greenhill, C.J., Majoros, A., Decker, T., Jenkins, B.J., and Mansell, A. (2014). STAT1 plays a role in TLR signal transduction and inflammatory responses. Immunol. Cell Biol. *92*, 761–769.

Lyko, F. (2018). The DNA methyltransferase family: a versatile toolkit for epigenetic regulation. Nat. Rev. Genet. *19*, 81–92.

Mackay, L.K., Minnich, M., Kragten, N.A.M., Liao, Y., Nota, B., Seillet, C., Zaid, A., Man, K., Preston, S., Freestone, D., et al. (2016). Hobit and Blimp1 instruct a universal transcriptional program of tissue residency in lymphocytes. Science *352*, 459–463.

Macosko, E.Z., Basu, A., Satija, R., Nemesh, J., Shekhar, K., Goldman, M., Tirosh, I., Bialas, A.R., Kamitaki, N., Martersteck, E.M., et al. (2015). Highly parallel genome-wide expression profiling of individual cells using nanoliter droplets. Cell *161*, 1202–1214.

Man, K., Miasari, M., Shi, W., Xin, A., Henstridge, D.C., Preston, S., Pellegrini, M., Belz, G.T., Smyth, G.K., Febbraio, M.A., et al. (2013). The transcription factor IRF4 is essential for TCR affinity-mediated metabolic programming and clonal expansion of T cells. Nat. Immunol. *14*, 1155–1165.

Martins, G., and Calame, K. (2008). Regulation and functions of Blimp-1 in T and B lymphocytes. Annu. Rev. Immunol. *26*, 133–169.

McGeachy, M.J., Stephens, L.A., and Anderton, S.M. (2005). Natural recovery and protection from autoimmune encephalomyelitis: contribution of CD4+CD25+ regulatory cells within the central nervous system. J. Immunol. *175*, 3025–3032.

Mombaerts, P., Iacomini, J., Johnson, R.S., Herrup, K., Tonegawa, S., and Papaioannou, V.E. (1992). RAG-1-deficient mice have no mature B and T lymphocytes. Cell *68*, 869–877.

Neumann, C., Heinrich, F., Neumann, K., Junghans, V., Mashreghi, M.-F., Ahlers, J., Janke, M., Rudolph, C., Mockel-Tenbrinck, N., Kühl, A.A., et al. (2014). Role of Blimp-1 in programing Th effector cells into IL-10 producers. J. Exp. Med. *211*, 1807–1819.

O'Connor, R.A., Malpass, K.H., and Anderton, S.M. (2007). The inflamed central nervous system drives the activation and rapid proliferation of Foxp3+ regulatory T cells. J. Immunol. *179*, 958–966.

Ogawa, C., Bankoti, R., Nguyen, T., Hassanzadeh-Kiabi, N., Nadeau, S., Porritt, R.A., Couse, M., Fan, X., Dhall, D., Eberl, G., et al. (2018). Blimp-1 functions as a molecular switch to prevent inflammatory activity in Foxp3^{+}RORγt^{+} regulatory T cells. Cell Rep. *25*, 19–28.e5.

Ohkura, N., Hamaguchi, M., Morikawa, H., Sugimura, K., Tanaka, A., Ito, Y., Osaki, M., Tanaka, Y., Yamashita, R., Nakano, N., et al. (2012). T cell receptor stimulation-induced epigenetic changes and Foxp3 expression are independent and complementary events required for Treg cell development. Immunity *37*, 785–799.

Okano, M., Bell, D.W., Haber, D.A., and Li, E. (1999). DNA methyltransferases Dnmt3a and Dnmt3b are essential for de novo methylation and mammalian development. Cell *99*, 247–257.

Overacre-Delgoffe, A.E., Chikina, M., Dadey, R.E., Yano, H., Brunazzi, E.A., Shayan, G., Horne, W., Moskovitz, J.M., Kolls, J.K., Sander, C., et al. (2017). Interferon-γ drives T_{reg} fragility to promote anti-tumor immunity. Cell *169*, 1130–1141.e11.

Parekh, S., Ziegenhain, C., Vieth, B., Enard, W., and Hellmann, I. (2016). The impact of amplification on differential expression analyses by RNA-seq. Sci. Rep. *6*, 25533.

Polansky, J.K., Kretschmer, K., Freyer, J., Floess, S., Garbe, A., Baron, U., Olek, S., Hamann, A., von Boehmer, H., and Huehn, J. (2008). DNA methylation controls Foxp3 gene expression. Eur. J. Immunol. *38*, 1654–1663.

Polansky, J.K., Schreiber, L., Thelemann, C., Ludwig, L., Krüger, M., Baumgrass, R., Cording, S., Floess, S., Hamann, A., and Huehn, J. (2010). Methylation matters: binding of Ets-1 to the demethylated Foxp3 gene contributes to the stabilization of Foxp3 expression in regulatory T cells. J. Mol. Med. (Berl.) *88*, 1029–1040.

Robinson, J.T., Thorvaldsdóttir, H., Winckler, W., Guttman, M., Lander, E.S., Getz, G., and Mesirov, J.P. (2011). Integrative genomics viewer. Nat. Biotechnol. *29*, 24–26.

Roers, A., Siewe, L., Strittmatter, E., Deckert, M., Schlüter, D., Stenzel, W., Gruber, A.D., Krieg, T., Rajewsky, K., and Müller, W. (2004). T cell-specific inactivation of the interleukin 10 gene in mice results in enhanced T cell responses but normal innate responses to lipopolysaccharide or skin irritation. J. Exp. Med. *200*, 1289–1297.

Rubtsov, Y.P., Rasmussen, J.P., Chi, E.Y., Fontenot, J., Castelli, L., Ye, X., Treuting, P., Siewe, L., Roers, A., Henderson, W.R., Jr., et al. (2008). Regulatory T cell-derived interleukin-10 limits inflammation at environmental interfaces. Immunity *28*, 546–558.

Rubtsov, Y.P., Niec, R.E., Josefowicz, S., Li, L., Darce, J., Mathis, D., Benoist, C., and Rudensky, A.Y. (2010). Stability of the regulatory T cell lineage in vivo. Science *329*, 1667–1671.

Rutishauser, R.L., Martins, G.A., Kalachikov, S., Chandele, A., Parish, I.A., Meffre, E., Jacob, J., Calame, K., and Kaech, S.M. (2009). Transcriptional repressor Blimp-1 promotes CD8(+) T cell terminal differentiation and represses the acquisition of central memory T cell properties. Immunity *31*, 296–308.

Shapiro-Shelef, M., Lin, K.-I., McHeyzer-Williams, L.J., Liao, J., McHeyzer-Williams, M.G., and Calame, K. (2003). Blimp-1 is required for the formation of immunoglobulin secreting plasma cells and pre-plasma memory B cells. Immunity *19*, 607–620.

Shen, F.W., Saga, Y., Litman, G., Freeman, G., Tung, J.S., Cantor, H., and Boyse, E.A. (1985). Cloning of Ly-5 cDNA. Proc. Natl. Acad. Sci. USA *82*, 7360–7363.

Takeda, K., Kaisho, T., Yoshida, N., Takeda, J., Kishimoto, T., and Akira, S. (1998). Stat3 activation is responsible for IL-6-dependent T cell proliferation through preventing apoptosis: generation and characterization of T cell-specific Stat3-deficient mice. J. Immunol. *161*, 4652–4660.

Tang, W.W.C., Dietmann, S., Irie, N., Leitch, H.G., Floros, V.I., Bradshaw, C.R., Hackett, J.A., Chinnery, P.F., and Surani, M.A. (2015). A unique gene regulatory network resets the human germline epigenome for development. Cell *161*, 1453–1467.

Toker, A., Engelbert, D., Garg, G., Polansky, J.K., Floess, S., Miyao, T., Baron, U., Düber, S., Geffers, R., Giehr, P., et al. (2013). Active demethylation of the Foxp3 locus leads to the generation of stable regulatory T cells within the thymus. J. Immunol. *190*, 3180–3188.

Vasanthakumar, A., Moro, K., Xin, A., Liao, Y., Gloury, R., Kawamoto, S., Fagarasan, S., Mielke, L.A., Afshar-Sterle, S., Masters, S.L., et al. (2015). The transcriptional regulators IRF4, BATF and IL-33 orchestrate development and maintenance of adipose tissue-resident regulatory T cells. Nat. Immunol. *16*, 276–285.

Williams, L.M., and Rudensky, A.Y. (2007). Maintenance of the Foxp3-dependent developmental program in mature regulatory T cells requires continued expression of Foxp3. Nat. Immunol. *8*, 277–284.

Wing, K., Onishi, Y., Prieto-Martin, P., Yamaguchi, T., Miyara, M., Fehervari, Z., Nomura, T., and Sakaguchi, S. (2008). CTLA-4 control over Foxp3+ regulatory T cell function. Science *322*, 271–275.

Wu, C., Wang, X., Gadina, M., O'Shea, J.J., Presky, D.H., and Magram, J. (2000). IL-12 receptor beta 2 (IL-12R beta 2)-deficient mice are defective in IL-12-mediated signaling despite the presence of high affinity IL-12 binding sites. J. Immunol. *165*, 6221–6228.

Xin, A., Masson, F., Liao, Y., Preston, S., Guan, T., Gloury, R., Olshansky, M., Lin, J.-X., Li, P., Speed, T.P., et al. (2016). A molecular threshold for effector CD8(+) T cell differentiation controlled by transcription factors Blimp-1 and T-bet. Nat. Immunol. *17*, 422–432.

Yang, X.O., Nurieva, R., Martinez, G.J., Kang, H.S., Chung, Y., Pappu, B.P., Shah, B., Chang, S.H., Schluns, K.S., Watowich, S.S., et al. (2008). Molecular antagonism and plasticity of regulatory and inflammatory T cell programs. Immunity *29*, 44–56.

Yang, B.-H., Hagemann, S., Mamareli, P., Lauer, U., Hoffmann, U., Beckstette, M., Föhse, L., Prinz, I., Pezoldt, J., Suerbaum, S., et al. (2016). Foxp3(+) T cells expressing RORγt represent a stable regulatory T-cell effector lineage with enhanced suppressive capacity during intestinal inflammation. Mucosal Immunol. *9*, 444–457.

Yoshida, H., Hamano, S., Senaldi, G., Covey, T., Faggioni, R., Mu, S., Xia, M., Wakeham, A.C., Nishina, H., Potter, J., et al. (2001). WSX-1 is required for the initiation of Th1 responses and resistance to L. major infection. Immunity *15*, 569–578.

Yue, X., Trifari, S., Äijö, T., Tsagaratou, A., Pastor, W.A., Zepeda-Martínez, J.A., Lio, C.-W.J., Li, X., Huang, Y., Vijayanand, P., et al. (2016). Control of Foxp3 stability through modulation of TET activity. J. Exp. Med. *213*, 377–397.

Zhou, L., Lopes, J.E., Chong, M.M.W., Ivanov, I.I., Min, R., Victora, G.D., Shen, Y., Du, J., Rubtsov, Y.P., Rudensky, A.Y., et al. (2008). TGF-beta-induced Foxp3 inhibits T(H)17 cell differentiation by antagonizing RORgammat function. Nature *453*, 236–240.

Zhou, X., Bailey-Bucktrout, S.L., Jeker, L.T., Penaranda, C., Martínez-Llordella, M., Ashby, M., Nakayama, M., Rosenthal, W., and Bluestone, J.A. (2009). Instability of the transcription factor Foxp3 leads to the generation of pathogenic memory T cells in vivo. Nat. Immunol. *10*, 1000–1007.

STAR★METHODS

KEY RESOURCES TABLE

REAGENT or RESOURCE	SOURCE	IDENTIFIER
Antibodies		
CD4-PerCP-eF710 (RM4-5)	eBioscience	Cat#46-0042; RRID: AB_1834431
CD4-BV421 (GK1.5)	Biolegend	Cat#100437; RRID: AB_100437
KLRG1-PE-Cy7 (2F1)	eBioscience	Cat#25-5893; RRID: AB_1518768
GITR (CD357)-PE (DTA-1)	BD	Cat#558119; RRID: AB_647208
CD25-PB (PC61 5.3)	eBioscience	Cat#RM6028; RRID: AB_2556574
CD44-BV421 (IM7)	BD	Cat#563970; RRID: AB_2738517
CD62L-APC (MEL-14)	BD	Cat#553152; RRID: AB_398533
CD126-APC (D7715A7)	Biolegend	Cat#115811; RRID: AB_2296238
CD45.1-PE-Cy7 (A20)	eBioscience	Cat#25-0453; RRID: AB_469629
CD45.1-APC-eF780 (A20)	eBioscience	Cat#47-0453; RRID: AB_1582229
CD45.2-APC-eF780 (104)	eBioscience	Cat#47-0454; RRID: AB_1272175
CD45.2-BV421 (104)	Biolegend	Cat#109832; RRID: AB_2565511
CD90.1-AF647 (OX-7)	Biolegend	Cat#202508; RRID: AB_492884
Foxp3-eF450 (FJK-16 s)	eBioscience	Cat#48-5773; RRID: AB_1518813
Foxp3-PE (FJK-16 s)	eBioscience	Cat#72-5775; RRID: AB_469978
IL-10-APC (JES5-16E3)	BD	Cat#554468; RRID: AB_398558
IFN-γ-PE (XMG1.2)	BD	Cat#554412; RRID: AB_395376
IFN-γ-PECy7 (XMG1.2)	eBioscience	Cat#25-7311; RRID: AB_469680
IL-17A-PerCP-Cy5.5 (TC11-18H10)	BD	Cat#560666; RRID: AB_1937311
IL-17A-PE (TC11-18H10)	BD	Cat#559502; RRID: AB_397256
Ki67-AF647 (16A8)	Biolegend	Cat#652408; RRID: AB_2562139
Chemicals, Peptides, and Recombinant Proteins		
MOG35-55 peptide (MEVGWYRSPFSRVVHLYRNGK)	Auspep	N/A
SGI-1027	Sigma	Cat#SML1358
Deposited Data		
ATAC-seq	This paper	GEO: GSE121764
RNA-seq	This paper	ENA: PRJEB30787
Experimental Models: Organisms/Strains		
Mouse: B6.129S7-*Rag1*^{tm1Mom}/J	The Jackson Laboratory	JAX, Stock#:002216
Mouse: B6.SJL-Ptprc^{a} Pepc^{b}/BoyJ	The Jackson Laboratory	JAX, Stock#: 002014
Mouse: B6.PL-*Thy1*^{a}/CyJ (CD90.1)	V. Buchholz (Institute of Medical Microbiology, Immunology and Hygiene, TU Munich)	JAX, Stock#: 000406
Mouse: B6.Cg-Tg(*Prdm1*-EYFP)1Mnz/J	The Jackson Laboratory	JAX, Stock#:008828
Mouse: B6.129-*Prdm1*^{tm1Clme}/J (Prdm1$^{flox/flox}$)	The Jackson Laboratory	JAX, Stock#:008100
Mouse: B6.129S1-*Il12rb2*^{tm1Jm}/J	The Jackson Laboratory	JAX, Stock#:003248
Mouse: B6N.129P2-*Il27ra*^{tm1Mak}/J	The Jackson Laboratory	JAX, Stock#:018078
Mouse: B6.129S2-*Il6*^{tm1Kopf}/J	The Jackson Laboratory	JAX, Stock#:002650
Mouse: B6.129S(Cg)-*Stat1*^{tm1Dlv}/J	S. Kemmner (U. Heemann, Department of Nephrology, Technical University (TU) Munich)	JAX, Stock#: 012606
Mouse: B6.Cg-*Stat3*^{tm2Aki} x CD4 Cre	F. Greten (Institute for Tumor Biology and Experimental Therapy, Georg-Speyer Haus, Frankfurt)	N/A

(*Continued on next page*)

Continued

REAGENT or RESOURCE	SOURCE	IDENTIFIER
Mouse: C.129S2-*Stat4*^{tm1Gru}/J	M. Löhning (Department of Rheumatology and Clinical Immunology, Charité-Universitätsmedizin Berlin)	JAX, Stock#: 002826
Mouse: C57BL/6-Tg(*Foxp3*-DTR/EGFP)23.2Spar/Mmjax (DEREG)	T. Sparwasser (Hannover Medical School, Hannover)	JAX, Stock#: 32050
Mouse: B6.129(Cg)-*Foxp3*$^{tm4(YFP/icre)Ayr}$/J	The Jackson Laboratory	JAX, Stock#: 016959
Mouse: B6.Cg-Tg(Mx1-cre)1Cgn/J (Mx1-Cre)	The Jackson Laboratories	JAX, Stock#: 003556
Mouse: B6.Cg-Tg(Cd4-cre)1Cwi/BfluJ (CD4 Cre)	The Jackson Laboratories	JAX, Stock#: 022071
Mouse: *Il10*$^{tm1.1Roer}$ (*Il10*$^{flox/flox}$)	Roers et al., 2004	MGI:3521569
Mouse: *Il10*$^{flox/flox}$ x B6.129(Cg)-*Foxp3*$^{tm4(YFP/icre)Ayr}$/J (*Il10*$^{\Delta Foxp3}$)	This paper	N/A
Mouse: Foxp3$^{tm1(cre)Saka}$ (*'Foxp3 Cre'*)	M. Oukka (Department of Pediatrics, University of Washington, USA)	MGI:3812203
Mouse: Rosa26 RFP x Foxp3 Cre	T. Bopp (Institute of Immunology, Johannes Gutenberg University, Mainz)	N/A
Mouse: *Prdm1*$^{flox/flox}$ x Foxp3 Cre (*Blimp1*$^{\Delta Foxp3}$)	This paper	N/A
Mouse: *Dnmt3a*$^{flox/flox}$	Dr. En Li (Novartis Pharmaceutical Inc.)	N/A
Mouse: *Dnmt3a*$^{flox/flox}$ x Mx1-Cre (*Dnmt3a*$^{\Delta Mx1}$)	This paper	N/A

CONTACT FOR REAGENT AND RESOURCE SHARING

Further information and requests for resources and reagents should be directed to and will be fulfilled by the Lead Contact, Thomas Korn (thomas.korn@tum.de).

EXPERIMENTAL MODELS AND SUBJECT DETAILS

Animals

Prdm1.yfp (Blimp1 (YFP)) reporter mice (Rutishauser et al., 2009), *Rag1*$^{-/-}$ mice (Mombaerts et al., 1992), *Il12rb2*$^{-/-}$ mice (Wu et al., 2000), *WSX* (*Il27r*)$^{-/-}$ mice (Yoshida et al., 2001), *Prdm1*$^{flox/flox}$ (*Blimp1*$^{flox/flox}$) (Shapiro-Shelef et al., 2003), *Il6*$^{-/-}$ mice (Kopf et al., 1994), and congenic CD45.1 mice (Shen et al., 1985) were obtained from Jackson Laboratory. Treg conditional Blimp1-deficient mice did not develop spontaneous autoimmunity. DEREG mice (Lahl et al., 2007) were kindly provided by T. Sparwasser (Twincore, Hannover Medical School, Hannover, Germany). *Stat3*$^{flox/flox}$ (*Stat3*^{tm2Aki}) mice (Takeda et al., 1998) were a gift of F. Greten (Institute for Tumor Biology and Experimental Therapy, Georg-Speyer Haus, Frankfurt). *Stat1*$^{-/-}$ mice (Durbin et al., 1996) were kindly provided by S. Kemmner (U. Heemann, Department of Nephrology, Technical University (TU) Munich). *Stat4*$^{-/-}$ mice (Kaplan et al., 1996) were obtained from M. Löhning (Department of Rheumatology and Clinical Immunology, Charité-Universitätsmedizin Berlin). To generate mice with cell type-specific excision of *lox*P-flanked cassettes, mice with *lox*P-flanked alleles were bred with CD4 Cre (Tg(*Cd4-cre*)^{1Cwi}) mice (Lee et al., 2001) (from Jackson Laboratory) or with *Foxp3 Cre* mice (Wing et al., 2008) obtained on the C57BL/6 background from M. Oukka (Department of Pediatrics, University of Washington, USA). *Dnmt3a*$^{flox/flox}$ mice were originally obtained from Dr. En Li (Novartis) (Okano et al., 1999). *Dnmt3a*$^{-/-}$ mice were generated by breeding Dnmt3a$^{flox/flox}$ mice with Mx1-Cre mice (from The Jackson Laboratory). Deletion of the floxed *Dnmt3a* allele was induced by intraperitoneal injection of 250 μg polyI:C (Sigma, P1530) four times every other day. CD90.1 mice were provided by V. Buchholz (Institute for Medical Microbiology, Immunology and Hygiene, TU Munich). Rosa26 RFP (Luche et al., 2007) x *Foxp3 Cre* mice were kindly provided by Tobias Bopp (Institute of Immunology, Johannes Gutenberg University, Mainz). *Il10*$^{flox/flox}$ x *Foxp3 Cre* mice were generated in WEHI by crossing *Il10* $^{flox/flox}$ mice (Roers et al., 2004) to *Foxp3 Cre* mice (Rubtsov et al., 2008), both obtained from Jackson Laboratory. All mouse strains were on pure C57BL/6 background. Animals were kept in a specific pathogen-free facility at the Technical University of Munich or at the Walter and Eliza Hall Institute of Medical Research, Parkville, Australia. All experimental protocols were approved by the standing committee for experimentation with laboratory animals of the Bavarian state authorities or the animal ethics committee of the Walter and Eliza Hall Institute and carried out in accordance with the corresponding guidelines. 6-10 week old age and sex-matched mice were used for all experiments, except for those involving methylation analysis (see Method details), in which only male mice were used.

METHOD DETAILS

Generation of mixed bone marrow chimeras

For generation of mixed bone marrow chimeras, *Rag1*$^{-/-}$ mice at 6-8 weeks of age were used as recipients. The mice were irradiated at a total dose of 7 Gray with two times 3.5 Gray 3h apart. 5-10 × 10^6 donor bone marrow cells depleted of CD90.2$^+$ cells were injected *i.v.* into irradiated *Rag1*$^{-/-}$ recipients within 16-20 h post irradiation. The reconstituted mice were maintained on antibiotic water (Enrofloxacin, Bayer, 0.1 mg/ml) for 2 weeks after transplantation. The reconstitution of the hematopoietic compartment was checked 5-6 weeks post cell transfer in peripheral blood.

Induction of EAE

EAE was induced by subcutaneous immunization in the base of tail with 200 μg of MOG35-55 (MEVGWYRSPFSRVVHLYRNGK; Auspep, Tullamarine, Australia) in complete Freund's adjuvant containing 500 μg Mycobacterium tuberculosis H37Ra (Difco, Detroit, MI)) per mouse plus intravenous injection (*i.v.)* of 200 ng pertussis toxin (Sigma-Aldrich) on days 0 and 2 after immunization. Disease progress and severity were assessed as described before (Korn et al., 2008). The peak of disease was typically between 15 and 20 days post immunization.

Adoptive transfer of Treg cells

1.0 × 10^5 - 3.0 × 10^5 FACS-sorted Treg cells (CD4$^+$Foxp3 (GFP)$^+$) from mixed bone marrow chimeras were transferred into *Rag1*$^{-/-}$ recipients along with 0.5 × 10^6 - 1.5 × 10^6 naive conventional T cells (CD4$^+$CD25$^-$CD44$^-$).

Preparation of mononuclear cells from the central nervous system (CNS)

Mice were perfused through the left cardiac ventricle with phosphate-buffered saline. The forebrain and cerebellum were dissected and spinal cords flushed out with phosphate-buffered saline by hydrostatic pressure. CNS tissue was cut into pieces and digested with 2.5 mg/ml collagenase D (Roche Diagnostics) and 1 mg/ml DNaseI (Roche Diagnostics) at 37°C for 45 min. Mononuclear cells were isolated by passing the CNS tissue through a 70 μm cell strainer (BD Biosciences), followed by a percoll gradient (70%/37%) centrifugation. The cells were removed from the interphase, washed and resuspended in culture medium for further analysis.

Preparation of peripheral T cells

Peripheral CD4$^+$ T cells were enriched from pooled spleen and lymph node cells using anti-CD4 microbeads (Miltenyi Biotec) followed by magnetic separation. Subsequently, Blimp1 (YFP)$^-$ Treg cells and Blimp1 (YFP)$^+$ Treg cells were sorted from Blimp1 (YFP) reporter mice as CD4$^+$YFP$^-$CD25$^+$GITR$^+$ and CD4$^+$YFP$^+$CD25$^+$GITR$^+$, respectively. Naive CD4$^+$ T cells (CD4$^+$CD25$^-$CD44$^-$) or (CD4$^+$Foxp3 (GFP)$^-$CD44$^-$) were sorted on a FACS Aria III machine (B D Biosciences).

Cell culture

10% FCS containing DMEM supplemented with 5 X 10^{-5} M β-mercaptoethanol, 1 mM sodium pyruvate, non-essential amino acids, L-glutamine, 100 U/ml penicillin, and 100 μg/ml streptomycin was used as culture medium. Cells were cultured in 96 well U bottom plates (Corning) at 37°C/5% CO_2. 0.5 × 10^5 or 1.0 × 10^5 FACS-sorted Treg cells (CD4$^+$CD25$^+$GITR$^+$ or CD4$^+$Foxp3 (GFP)$^+$) were stimulated with anti-CD3 and anti-CD28 dynabeads (Invitrogen) for four days in the presence of either recombinant murine IL-2 (100 ng/ml) alone or with individual cytokines (recombinant murine); IL-6 (50 ng/ml) or IL-1β, IL-4, IL-10, IL-12, IL-17, IL-21, IL-23, IL-24, IL-27, IL-33 and IFN-γ (100 ng/ml). All cytokines were purchased from Miltenyi Biotec and R & D Systems. In some experiments, Treg cell cultures were treated with SGI-1027 (indicated concentrations) (Sigma Aldrich). For iTreg cell cultures, naive T cells (CD4$^+$Foxp3 (GFP)$^-$CD62L$^+$CD44$^-$) were sorted from Foxp3 (GFP) reporter mice and cultured with anti-CD3 and anti-CD28 dynabeads for five days in the presence of IL-2 (10 ng/ml) and TGF-β (5 ng/ml; R & D Systems).

Antibodies and flow cytometry

Cell suspensions from lymphoid organs were stained with fluorochrome-conjugated anti-mouse CD4 (RM4-5), CD25 (PC61.5), CD44 (IM7), CD45.1 (A20), CD45.2 (104), CD62L (MEL-14), CD90.1 (OX-7), GITR (CD357) (DTA-1), Ki67 (16A8), CD126 (D7715A7) and KLRG1 (2F1), which were purchased from either Biolegend, eBioscience or BD Biosciences. For dead cell exclusion, LIVE/DEAD® fixable Near-IR stain kit (Invitrogen) was used. For intracellular staining, Foxp3 staining kit (eBioscience) was used for Foxp3 (FKJ-16 s), IL-10 (JES5-16E3), IL-17 (TC11-18H10), IFN-γ (XMG1.2). For cytokine stainings, cells were stimulated in culture medium containing phorbol 12-myristate 13-acetate (PMA, 20 ng/ml, Sigma), ionomycin (1 μg/ml, Sigma), and monensin (GolgiStop 1 μl/ml, BD Biosciences) at 37°C/5% CO_2 for 4 h. Flow cytometric analysis was performed on a CyAn ADP flow cytometer (Beckman Coulter) or a FACS Aria III (BD Biosciences), and flow cytometric data were analyzed using FlowJo software (Tree Star).

Quantitative PCR

Total RNA was isolated from purified Treg cells and Tconv cells with RNAeasy Plus micro kit (QIAGEN). The isolated RNA was transcribed into cDNA using the TaqMan Reverse Transcription Reagents Kit (Life Technologies) according to the manufacturer's instructions. Probes were purchased from Life Technologies and the assays were performed on 96-well reaction plates (Life

Technologies). The real time PCR was performed on StepOnePlus system (Life Technologies). In all experiments *Actb* was used as reference gene to normalize gene expression.

RNA-seq

Total RNA was isolated from purified Treg cells and Tconv cells with RNAeasy Plus micro kit (QIAGEN). Quality and integrity of total RNA was controlled on Agilent Technologies 2100 Bioanalyzer (Agilent Technologies). RNaseq analysis: library preparation for bulk 3′-sequencing of poly(A)-RNA was done as described previously (Parekh et al., 2016). Briefly, barcoded cDNA of each sample was generated with a Maxima RT polymerase (Thermo Fisher) using oligo-dT primer containing barcodes, unique molecular identifiers (UMIs) and an adaptor. 5′ ends of the cDNAs were extended by a template switch oligo (TSO) and full-length cDNA was amplified with primers binding to the TSO-site and the adaptor. cDNA was tagmented with the Nextera XT kit (Illumina) and 3′ end-fragments finally amplified using primers with Illumina P5 and P7 overhangs. In comparison to Parekh et al. (2016), the P5 and P7 sites were exchanged to allow sequencing of the cDNA in read1 and barcodes and UMIs in read2 to achieve a better cluster recognition. The library was sequenced on a NextSeq 500 (Illumina) with 75 cycles for the cDNA in read1 and 16 cycles for the barcodes and UMIs in read2. Data was processed using the published Drop-seq pipeline (v1.0) to generate sample- and gene-wise UMI tables (Macosko et al., 2015). Reference genome (GRCm38) was used for alignment. Transcript and gene definitions were used according to the ENSEMBL annotation release 75. Differential gene expression was calculated using the DESeq2 package (v1.18.0) (Love et al., 2014). We focused on genes with less than 5% probability to be false positive (p-adjusted < 0.05). When necessary, log2 transformation was realized using ''rlog'' function from Deseq2.

For gene set enrichment analysis (GSEA) a ranked list of the fold change of RNA-seq read values of the samples to be compared was calculated. The java GSEA Desktop Application v2.2.1, was used in conjunction with the Molecular Signatures Database v45.1 to run the analysis. We always used sample label (phenotype) permutation and thus applied an FDR of 0.25.

ChIP-seq

To assess Blimp1 binding at specific gene loci, we interrogated the ChIP-seq data published earlier (Mackay et al., 2016). Here, $CD8^+$ T cells from *Blimp1*-Bio mice carrying a biotin acceptor sequence at the carboxyl terminus of Blimp1, which was biotinylated *in vivo* by coexpression of the *Escherichia coli* biotin ligase BirA from the $Rosa26^{BirA}$ allele, were stimulated *in vitro* with anti-CD3 and anti-CD28 in the presence of IL-2 and IL-12 (Mackay et al., 2016). To obtain STAT3 ChIP-seq data, murine naive $CD4^+$ T cells were stimulated with anti-CD3 and anti-CD28 in the presence of IL-6 (Hirahara et al., 2015). ChIP-seq tracks were generated using Integrated genome browser (Robinson et al., 2011).

ATAC-seq

ATAC-seq was done as described by Corces et al., (2017). Briefly, 50000 cells (viability > 90%) were pelleted (500 *rcf.*, 4°C, 5 min) and re-suspended in ATAC Resuspension Buffer (10mM Tris-HCl pH 7.4, 10mM NaCl, 3mM $MgCl_2$) supplemented with 0.1% NP40, 0.1% Tween-20 and 0.01% digitonin for lysis, incubated on ice for 3 min and then 1ml of ATAC Resuspension Buffer supplemented only with 0.1% Tween-20 was added and spun at 500 g for 10 min at 4°C to collect nuclei. Nuclei were subsequently re-suspended in 50 μl Transposase reaction containing 25μL 2x tagmentation buffer, 5.25 μl water, 2.5 μl Tn5 Transposase (Illumina Nextera DNA Library Preparation Kit, cat. FC-121-1030), 16.5 μl PBS, 0.25 μl of 2% digitonin (Promega, G9441), 0.5 μl of 10% Tween-20. Reactions were incubated for 30 min at 37°C in a thermomixer shaking at 900 rpm and DNA purified using QIAGEN PCR clean-up MinElute kit (QIAGEN). The transposed DNA was subsequently amplified in 50μl reactions with custom primers as described (Buenrostro et al., 2013). After 4 cycles libraries were then monitored with qPCR: 5 μl PCR sample in a 15 μl reaction with the same primers. qPCR output was monitored for the ΔRN; 0.25 ΔRN cycle number was used to estimate the number of additional cycles of the PCR reaction needed for the remaining PCR samples. Amplified libraries were purified with the QIAGEN PCR clean-up MinElute kit (QIAGEN) and size selected for fragments less than 600 bp using the Agencourt AMPure XP beads (Beckman Coulter). Libraries were quality controlled by Qubit and Agilent DNA Bioanalyzer analysis. Deep sequencing was performed on a HiSeq 1500 system according to the standard Illumina protocol for 50bp single-end reads.

ATAC-seq reads were aligned to the mouse genome mm10 using Bowtie (Langmead, 2010) with options ''-q -n 2–best–chunkmbs 2000 -p 32 -S.'' ATAC peaks over Input background were identified using Homer (Heinz et al., 2010) findPeaks.pl with option ''-style factor.'' Peaks from all samples were merged using mergePeaks resulting in a unified Peak set. The peak list was filtered for promoter-associated peaks (distance to TSS < 1000bp) with bedtools. Raw ATAC coverage counts were then calculated with annotatePeaks within 500bp across the peak centers. Differential ATAC peaks were determined with the DESeq2 result function and filtered for padj < 0.05. Genomic feature annotation of ATAC-seq peaks was done using annotatePeaks. Transcription factor motif prediction was done with Homer findMotifsGenome.pl.

Methylation analysis

For all methylation analyses, cells from male mice were used. Bisulfite-converted DNA was prepared from FACS-sorted Treg cells and Tconv cells according to the manufacturer's instructions (EZ DNA Methylation-Direct Kit, Zymo Research). Pyrosequencing was performed as described previously (Yang et al., 2016). Amplification and sequencing of the Treg cell-specific demethylated region (TSDR) (chromosome position X:7583986-7584149), the *Foxp3* promoter (chromosome position X:7579550-7579731), a region in

Ctla4 (chromosome position 1:60912472-60912685), *Coro2a* (chromosome position 4:46567312-46567503), *Nfkbiz* (chromosome position 16:55836298-55836608) and *Ikzf3* (chromosome position 11:98476715-98477042) was performed with the following amplification/sequencing primer sets: mTSDR-for, biotinylated (5′-TAAGGGGGTTTTAATATTTATGAGGTTT-3′), mTSDR-rev (5′-CCTAAACTTAACCAAATTTTTCTACC-3′), mTSDR-S1 (5′-ACCCAAATAAAATAATATAAATACT-3′), mTSDR-S2 (5′-ATCTACCCCACAAATTT-3′), mTSDR-S3 (5′-AACCAAATTTTTCTACCATT-3′), mFoxp3Pr-for (5′-GTTTATTTTGGTGAAGTGGATTGTTAGAGG-3′), mFoxp3Pr-rev, biotinylated (5′-CCCTACAATTATCAACACACACACTCAT-3′), mFoxp3Pr-S1 (5′- TTTGTGGGAAATTGTTATATTATTAAA-3′), mCTLA4-for (5′-AGTGGTGTTGGTTAGTAGTTATGG-3′), mCTLA4-rev, biotinylated (5′-ACATAAATTCCACCTTACAAAAATACAAT-3′), mCTLA4-S1 (5′-GTTGGTTAGTAGTTATGGT-3′), mCTLA4-S2 (5′-TTATTATTATATAATATTGATGAGG-3′), mCTLA4-S3 (5′-GATAAATGATTAAATGATTGAGG-3′), mCTLA4-S4 (5′-ATTTTATTATTTAAGGATTGAGAG-3′), mCoro2a-for (5′- GGTTTTTTGAATTATTTTGAGTTGTTAGAA-3′), mCoro2a-rev, biotinylated (5′- CCTACTCCTTACAAAATAAACCTTACTA-3′), mCoro2a-S1 (5′- TTTGAGTTGTTAGAATTTATAAAA-3′), mNfkbiz-for (5′- TGAAGGAAAAGGGGATAAATTTGT), mNfkbiz-rev, biotinylated (5′- CTTAAAAACATTCACCCACTTACC-3′), mNfkbiz-S1 (5′- GGATTTTGATTTTTAGGGATG-3′), mNfkbiz-S2 (5′- ATTTTGAGGTTTATGTTGAAT-3′), mIkzf3-Ex7-for (5′- AAGTGTGGAGGTAAGATATATTAAAGT-3′), mIkzf3-Ex7-rev, biotinylated (5′- ACCAAATACTCCCCTATTCTTTAACTA-3′), mIkzf3-Ex7-S1 (5′- GGATAGATTAGTAAGTAATGTGGTTA-3′), mIkzf3-Ex7-S2 (5′- AGTAGATATTTTGGATGAGATAATATAG-3′). The indicated chromosome positions refer to genome assembly GRCm38.p5.

QUANTIFICATION AND STATISTICAL ANALYSIS

Statistical evaluations of cell frequency measurements, cell numbers, mRNA amounts, and protein levels were performed with the unpaired Student's t test when two populations were compared. Two-tailed p values < 0.05 were considered significant. Multiple comparisons were performed with one-way ANOVA or two-way ANOVA followed by post hoc multiple comparisons tests as indicated in the legends to the figures. EAE scores between groups were analyzed as disease burden per individual day with one-way-ANOVA and post hoc test as indicated. Survival curve was calculated using Kaplan-Meier analysis and the p values were analyzed with log-rank test (Mantel-Cox). A p value of $p < 0.05$ was considered significant. Calculations were performed using Graph Pad Prism v5.0 (Graph-Pad software).

DATA AVAILABILITY

The data that support the findings of this study are available from the corresponding author upon request. Accession codes: The RNA-seq data are available at https://www.ebi.ac.uk/ena under the accession code ENA: PRJEB30787. The ATAC-seq data are available at https://www.ncbi.nlm.nih.gov/geo under the accession code GEO: GSE121764.